Marine Structures 79 (2021) 103050

Contents lists available at ScienceDirect

Marine Structures

journal homepage: www.elsevier.com/locate/marstruc

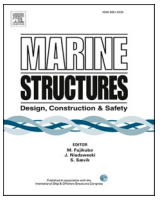

Methodology for developing a response-based correction factor (alpha-factor) for allowable sea state assessment of marine operations considering weather forecast uncertainty

Mengning Wu [a,*], Zhen Gao [a,b,c]

[a] Department of Marine Technology, Norwegian University of Science and Technology (NTNU), Trondheim, NO-7491, Norway
[b] Centre for Autonomous Marine Operations and Systems (AMOS), NTNU, Trondheim, NO-7491, Norway
[c] Centre for Marine Operations in Virtual Environments (MOVE), NTNU, Trondheim, NO-7491, Norway

ARTICLE INFO

Keywords:
Marine operations
Weather forecast
Forecast uncertainty quantification
Allowable sea states
Weather windows
Wind turbine installation

ABSTRACT

The concept of the alpha-factor, a correction factor on the significant wave height limit, was developed by DNV to consider the effect of weather forecast uncertainty in planning and executing marine operations. In this paper, a new defined response-based correction factor, called the response-based alpha-factor α_R, is proposed to account for the forecast uncertainty of both significant wave height H_s and peak wave period T_p, and quantify their effect on dynamic response of offshore structures. A general methodology for developing α_R for the use in assessing allowable sea states for marine operations is presented, with emphasis on considering the effect of the weather forecast uncertainty. It consists of uncertainty quantification of the sea state forecast, statistical analysis of dynamic responses of the coupled system for marine operations and allowable sea state assessment using response-based criteria. Based on the methodology, α_R for an operation can be derived, in terms of the ratio between the characteristic values of the operational limiting response parameter in the condition with or without the weather forecast uncertainty. Then, the allowable sea states can be assessed in terms of the forecast lead time, to include the effect of the weather forecast uncertainty on the operation decision-making. The workable weather windows can finally be identified and selected through a comparison between the allowable sea states and weather forecasts in the execution phase. Followed by the detailed description of the proposed methodology, a case study dealing with single blade installation for offshore wind turbine using a semi-submersible crane vessel is conducted. The crane tip motion is regarded as the operational limiting response parameter to illustrate the methodology based on frequency-domain response analysis approach. The uncertainty in sea state forecasts generated by two machine learning-based forecasting methods is considered in this paper. Results show that in addition to the forecast uncertainty of H_s, that of T_p also requires to be addressed for marine operations with floating structures (such as the semi-submersible crane vessel). The proposed method provides an efficient way to incorporate the weather forecast uncertainty into the allowable sea states assessment for marine operations. The obtained allowable sea states can provide a good reference for the decision-making of the operation in the execution phase.

* Corresponding author.
E-mail address: mengning.wu@ntnu.no (M. Wu).

https://doi.org/10.1016/j.marstruc.2021.103050
Received 23 February 2021; Received in revised form 11 June 2021; Accepted 24 June 2021
Available online 1 July 2021

1. Introduction

The gradual transition away from fossil fuels towards a carbon-neutral society is one of the greatest challenges of the 21 century [1]. Over the past decade, renewable energy, such as wind energy and solar energy, is the fastest-growing energy source globally. Among them, offshore wind energy is identified as one of the most promising sources [2] since it is more stable and stronger, not being exhausted and produce no emissions, and it becomes also one of the cheapest ways of generating electricity from renewable energy. To access wind energy in deep waters and farther offshore locations, the demand of related marine operations such as the offshore wind turbine installation has increased dramatically. According to the definition in Det Norske Veritas (DNV) [3], marine operations are generally classified as either weather-restricted or weather-unrestricted, depending on the duration of the operation. Marine operations with the duration less than 72 h, mainly focused in this paper, are typically defined as weather-restricted operations. Normally, the decision for weather-restricted operations during the execution phase is made in terms of the workable weather window. The workable weather window represents the duration during which the forecast sea states (typically characterized by significant wave height H_s and peak wave period T_p) are lower than the allowable sea states for an operation, indicating that the operation can be performed safely. The sea states leading to the characteristic value of a limiting response parameter of the operation lower than its allowable limit are the allowable sea states. Guachamin-Acero et al. [4] proposed a general methodology to determine allowable sea states for marine operations and applied it to the installation of monopile [5], transition piece [6,7] and tower and rotor nacelle assemblies (RNAs) [8] for offshore wind turbine, by identifying critical events and studying responses of corresponding limiting response parameters derived from numerical simulations. Several other works [9–11] have also been carried out to assess allowable limits for different marine operations. In addition to the allowable sea states, the forecasted sea state is another important parameter for decision-making in the execution phase of marine operations. At present, there are generally three types of sea state forecasting methods, namely the physics-based numerical method, the statistical method and the machine learning method. The physics-based numerical method utilizes the wave energy balance equation with various physical processes to simulate the process of wave evolution and solve the equation through numerical techniques. Strong physical background of the equation guarantees the reliable of the method, and some models based on the method have been widely used, such as WAM (wave modeling) [12], SWAN (simulating wave nearshore) [13] and WaveWatch III [14]. However, large computational cost of it has stimulated the development of other methods. The statistical method and the machine learning method do not consider physical phenomena in waves, but make forecast purely based on the relationship between data in the long-term historical time series. Both of them have high computational efficiency. Commonly used statistical-based models for wave forecasting include the autoregressive model [15,16], ARMA (autoregressive moving average) model [16,17], ARIMA (autoregressive moving average) model [17–19], etc. For the machine learning method, several neural networks have been widely used, such as ANN (artificial neural network) [20–23], RNN (recurrent neural network) [24,25] and ANFIS (adaptive-network-based neural network) [26–29].

Accurate weather forecasts can improve the reliability of the weather window identification and can potentially save massive installation and operational costs. However, it is well known that there is inherent uncertainty in weather forecasts, no matter which method is employed. As a consequence, how to quantify the uncertainty in weather forecasts and how to reflect this uncertainty when planning and executing marine operations thus become a key issue. So far, only a few studies have been published on investigating the effect of weather forecast uncertainty on marine operations. At present, an alpha-factor α [30] (a normalized factor less than 1), proposed by DNV, is normally used to address the uncertainty in weather forecasts when performing marine operations. It is determined by evaluating H_s forecasts and the aim of it is to reduce the design limit of H_s to a certain extent and therefore making the operation more conservative. In practical applications, DNV [3,13] provides tabulated α-factors for European waters, allowing users to select one for weather-restricted operations in terms of the operational period, design wave height, the quality of weather forecasts, etc. The selected factor can subsequently be used to correct the allowable sea state (in terms of H_s) to include the weather forecast uncertainty. Following this method, a similar study was carried out by Wilcken [31] to generate alpha-factors in the Barents Sea.

Although tabulated alpha-factors for H_s are explicitly given in the standard, it does not provide tabulated alpha-factors for other wave variables. It is well known that floating offshore structures are increasingly used for marine operations, and such structures are highly sensitive to the wave period. For marine operations involving floating systems, forecast uncertainty in wave periods such as the peak wave period T_p is also important and should be taken into account. Furthermore, the alpha-factor is completely derived from sea state variables without considering the characteristics of different offshore structures. In other words, it is independent of the type and physical limits of marine operations. However, the failure of marine operations is in principle related to the response of offshore structures and equipment. Their extreme response essentially decides whether a specific operation can be performed or not during the execution phase. Gintautas, T, and Sørensen, J. D [32]. considered weather forecast uncertainty by applying ensemble weather forecasts to simulate an offshore lift operation and whether the operation should be performed or not is decided based on the comparison between the responses with the related physical limitations. However, physical indicators are not convenient to directly guide the decision-making.

Under these circumstances, it is necessary to define an operation-based factor to quantify forecast uncertainties in both H_s and T_p for marine operations. In this paper, a correction factor, called the response-based alpha-factor α_R, is proposed to reflect the effect of forecast uncertainties in sea states on marine operations. It is similar to the alpha-factor but can address forecast uncertainties in both H_s and T_p and depends on the type and the response of operations. The design principle of the α_R is to ensure that the safety level (i.e., the target failure probability) of the operation is the same with and without weather forecast uncertainty. It is derived by the quantification of weather forecast uncertainty, numerical modeling of structural dynamic responses and probabilistic analysis of extreme responses for a certain operation. Based on the α_R, a methodology is presented to assess the allowable sea states for marine operations, with emphasis on considering weather forecast uncertainty. Followed by the methodology, the allowable sea sates

including weather forecast uncertainty of weather-restricted marine operations can be assessed, and the workable weather windows can be further identified and selected.

The paper consists of the following sections. A brief introduction of the alpha-factor proposed by DNV is presented in Section 2. Section 3 provides a detailed description of the proposed methodology for developing the response-based alpha-factor. The key parameters and framework of the methodology are described in Section 3.1 and 3.2 respectively. Subsequently, involved analytical techniques, i.e., forecast uncertainty quantification, extreme response analysis and α_R derivation are given in Section 3.3, 3.4 and 3.5, respectively. Furthermore, the usage of the derived α_R is briefly introduced in Section 3.6. In Section 4, a case study of offshore wind turbine blade installation using a semi-submersible crane vessel is conducted, to demonstrate the feasibility of the proposed methodology and to illustrate the procedure. A brief introduction of the study area and utilized two machine learning-based forecasting methods (i.e., the time-series-based machine learning (TSML) method and the physics-based machine learning (PBML) method) is given in Section 4.1. Section 4.2 provides the uncertainty analysis of weather forecasts. The motion response analysis, the response-based alpha-factor generation and allowable sea states assessment with respect to the crane tip motion are summarized and analyzed in Sections 4.3, 4.4 and 4.5, respectively. Finally, the conclusions are made in Section 5.

2. Alpha-factor proposed by DNV

A brief introduction of the alpha-factor proposed by DNV [30] is given below. The alpha-factor α is estimated by dividing the maximum wave height with a defined probability level to the same level maximum wave height with H_s forecast uncertainty. The expression is shown in Eq. (1).

$$\alpha = \frac{H_{max}}{H_{\max\_WF}} \tag{1}$$

where $H_{\max}$ is the characteristic value of maximum wave height, that is defined as the extreme wave height during a given reference period (e.g. 3 h) with an exceedance probability of 10^{-4}. $H_{\max\_WF}$ is the characteristic value of maximum wave height with the same exceedance probability taking into account the forecast uncertainty in H_s. For clarity, the symbols H_s^t and H_s^f are used to denote the actual (true) and forecasted value of H_s in the following introduction, respectively.

When a forecasted H_s^f value is given and its forecast uncertainty is not considered, it can be regarded as the true H_s, i.e., H_s^t. Then the probability density function (PDF) of maximum wave height with the given significant wave height is defined as $f_{H|H_s^t}(h'|h_s^t)$. Based on the cumulative distribution function (CDF) of maximum wave height (see Eq. (2)), the characteristic value $H_{\max}$ can thereby be calculated by Eq. (3).

$$F_H(h) = \int_0^h f_{H|H_s^t}(h'|h_s^t)dh' \tag{2}$$

$$1 - F_H(H_{\max}) = 10^{-4} \tag{3}$$

By contrast, when forecast uncertainty in H_s^f is considered, the conditional PDF of H_s^t with given forecasted value H_s^f has to be taken into account, to show all possible true H_s and the corresponding individual wave height distribution. As a result, a joint PDF of H and H_s^t is established as

$$f_{HH_s^t}(h', h_s^t) = f_{H|H_s^t}(h'|h_s^t) \cdot f_{H_s^t|H_s^f}(h_s^t|h_s^f) \tag{4}$$

where $f_{H|H_s^t}(h'|h_s^t)$ is the conditional PDF of maximum wave height with a given actual significant wave height, which is described above. $f_{H_s^t|H_s^f}(h_s^t|h_s^f)$ is the conditional PDF of actual significant wave height given a forecasted significant wave height, that is obtained from the uncertainty analysis of the forecast model.

Through integration, the marginal CDF of the maximum wave height can be obtained, as shown in Eq. (5).

$$F_H^{WF}(h) = \int_0^h \int_0^{+\infty} f_{H|H_s^t}(h'|h_s^t) \cdot f_{H_s^t|H_s^f}(h_s^t|h_s^f) dh_s^t dh' \tag{5}$$

In Eq. (5), it is important to quantify the weather forecast uncertainty and establish $f_{H_s^t|H_s^f}(h_s^t|h_s^f)$. In the previous technical report of the joint industry project (JIP) [30], the forecast uncertainty of H_s is characterized by the forecast error H_s^e, which is defined as Eq. (6). H_s^e is a random variable which is assumed to follow a Gaussian distribution. According to Eq. (6), $f_{H_s^t|H_s^f}(h_s^t|h_s^f)$ can be transformed from the relevant error distribution. This means that its mean value is the forecasted significant wave height adjusted by the error bias and its standard deviation is the same as that of the forecast error. However, it is important to emphasize that the forecast uncertainty can be also defined in other ways. Subsequently, the characteristic value $H_{\max\_WF}$ can be determined by solving Eq. (7), which is used to generate the α-factor for the given H_s^f by Eq. (1) together with $H_{\max}$.

$$H_s^e = H_s^f - H_s^t \tag{6}$$

$$1 - F_H^{WF}(H_{\max\_WF}) = 10^{-4} \tag{7}$$

Following the above procedure, α-factors can be estimated and tabulated for different weather forecast scenarios. Although the alpha-factor is obtained based on the extreme wave height, it is used as a ratio of the significant wave height for marine operations, assuming that the extreme wave height is proportional to the significant wave height and disregarding the effect of wave period and system responses. In practice, for the execution phase of an operation, the specific alpha-factor needs to be selected from the tabulated values in terms of the operation duration, the forecast lead time, the quality of weather forecasts, etc. This selected factor can then be used to correct the allowable H_s (H_{s_lim}) of the operation by Eq. (8) to include the weather forecast uncertainty.

$$H_{s\_\mathrm{lim}\_\alpha} = \alpha \cdot H_{s\_\mathrm{lim}} \tag{8}$$

where $H_{s\_\mathrm{lim}\_\alpha}$ is the new limit H_s accounting for the forecast uncertainty. In real marine operations, the forecasted value of H_s will be compared to this new H_s limit to determine whether a safe operation can be performed. If the forecasted H_s is smaller than the new H_s limit, the marine operation can be safely performed.

3. Response-based alpha-factor

In this section, the methodology for derivation of the response-based alpha-factor α_R is proposed and introduced. Its purpose is to consider the effect of forecast uncertainties in sea states (i.e., H_s and T_p) on marine operations from a perspective of the system responses. A detailed description of the methodology framework, the key parameters as well as different related analytical techniques are introduced in the following subsections.

3.1. Key parameters

Considering the properties of marine operations and weather forecasting, the α_R is presented as a function of:

1) The type of marine operation and the relevant operational limiting response parameter
2) The duration T_E of the selected operation, i.e. the time used in the extreme response analysis. The characteristic value of the extreme response used to define and calculate the response-based alpha-factor is the value with a certain exceedance probability (e.g., 10^{-4} or 10^{-2}).
3) The sea state reference period T_R, e.g. 1 h, 3 h, etc., is the period used to define a stationary sea state, to quantify the forecast uncertainty and to derive the allowable sea states. It is also the same period that α_R will be applied in marine operations to correct the allowable sea states when forecast uncertainty is considered.
4) The forecast variable of weather conditions, e.g. H_s, T_p, etc.
5) The weather forecasting method
6) The lead time T_L of weather forecasts (i.e. the forecast horizon)
7) The forecast uncertainty model

Among the above factors, the type of marine operation must first be selected. The specific operation decides the critical events during the operation and the relevant operational limiting response parameters. Regarding the method for identification of critical events and limiting parameters, refer to Guachamin-Acero et al. [4]. By means of the numerical modeling of the selected operation during the operational duration T_E, the dynamic responses of the limiting parameters can be studied. The corresponding extreme value distribution and the characteristic value can therefore be determined by statistically analyzing the dynamic responses. For operations such as offshore wind turbine blade installations, the critical event may be more concentrated in the final mating phase between blade root and turbine hub opening. T_E is only a few minutes in this case, and the extreme response should be analyzed from the numerical simulation with such short period. In contrast, for operations such as towing operation and sea transports, they generally take several hours/days, and the numerical simulations with a long time are needed to cover the whole period. In such cases, it is more complicated. One needs to deal with the sequence of the sea states during operation and the worst sea state might be considered to achieve a conservative result.

Regarding weather conditions, T_R refers to a time interval in which the sea state can be assumed to be stationary. In this period, the statistics (such as the mean value and standard deviation) of a realization of the wave elevation are considered to be independent of time. For marine operations, T_R is normally 1 h or 3 h. The other three factors, i.e. the forecast variable of weather conditions, the weather forecasting method and the lead time T_L of weather forecasts, determine the uncertainty related to the weather forecasts. Regarding the forecast variable, significant wave height H_s and peak wave period T_p which are utilized to describe sea states are considered. It should be pointed out that for operations sensitive to wind load, uncertainty in the wind forecast may also be included and related variables (e.g., mean wind speed U_w) can be regarded as another forecast variable. With regard to the lead time T_L, it could range from one- or three-hours-ahead (depending on T_R) to several-days-ahead, taking into account the execution time of the selected marine operations. As for the forecasting method, different methods (e.g., physics-based numerical method, statistical method or machine learning method) can be adopted to generate forecasts. For instance, Wu et al. [29,33] developed different machine

learning-based methods for multi-step-ahead forecasting of wave conditions. In addition, physics-based forecast products provided by various institutes such as the European Center for Medium-Range Weather Forecasts (ECMWF) [34–36], the Norwegian Meteorological Institute (MET-Norway) [37] and the National Center for Environmental Prediction (NCEP) [38] can be used if available. After obtaining weather forecasts, a forecast uncertainty model is utilized to quantify uncertainties in sea state forecasts.

3.2. Framework

The procedure to derive α_R is introduced in this section. The framework of the proposed methodology is illustrated in Fig. 1 and described in the following steps.

Weather forecast and uncertainty quantification

1. First of all, determine the weather variable that needs to be forecasted, the sea state reference period T_R and the lead time T_L.
2. Follow by the above decision, the weather conditions are then forecasted through the physics-based numerical method (such as WAM and SWAN), the statistical method (such as ARIMA) or the machine learning method (such as ANN and ANFIS). The weather forecasting is carried out for both H_s and T_p in this study, which are utilized to describe the sea state. In order to better illustrate the weather forecast analysis, the actual sea state is termed as (H_s^t, T_p^t) and the forecasted sea state is presented as (H_s^f, T_p^f). Normally, for the forecast uncertainty analysis, the forecasted data should be as much as possible.
3. Afterwards, the forecast uncertainty should be quantified. Similar to the alpha-factor method, this can be done by analyzing the statistical characteristics of a pre-defined forecast error factor in terms of T_L.
4. Finally, for a given forecasted sea state (H_s^f, T_p^f), the distribution of the actual sea state (H_s^t, T_p^t) can be established by transforming the error distribution. This distribution reflects all possible true sea states for a given forecast value, and illustrates the weather forecast uncertainty. The method and details for forecast uncertainty quantification will be presented in Section 3.3.

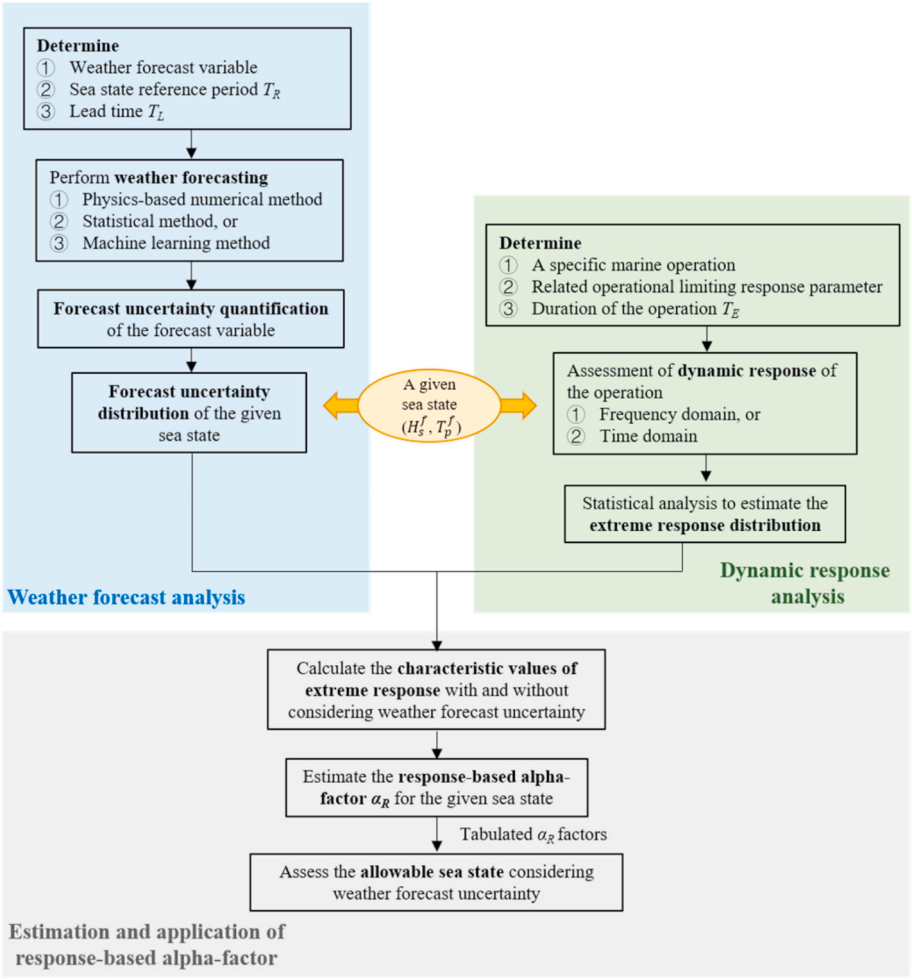

Fig. 1. The framework of the response-based alpha-factor method.

Dynamic response analysis

1. For dynamic response analysis, a specific marine operation should be determined first. For this operation, the critical events and operational limiting response parameters as well as the operational duration T_E should then be identified accordingly.
2. Afterwards, for the given sea state concerned in the weather forecast analysis, the dynamic response of the limiting response parameter can be simulated and assessed based on frequency- or time-domain response analysis approaches. This depends on the properties of the selected operation.
3. Finally, by statistically analyzing the dynamic responses, the extreme response distribution can be estimated. A description of the extreme response analysis will be given in Section 3.4.

Estimation and application of the response-based alpha-factor

1. Once the forecast uncertainty distribution and the extreme response distribution for a given sea state (H_s^f, T_p^f) are determined, the characteristic values of the limiting parameter in the condition with and without considering weather forecast uncertainty can be calculated respectively. The characteristic value corresponds to the extreme response for a target exceedance probability (e.g., 10^{-4}) of the extreme response distribution within the period T_E.
2. By dividing two calculated values, the α_R for this given sea state can be estimated. The details for calculating the α_R will be presented in Section 3.5.
3. Followed by this procedure, the tabulated α_R can be generated for various sea states. Based on it, the allowable sea states associated with the operation can be assessed, in order to account for the weather forecast uncertainty. This will be discussed in Section 3.6.

3.3. Uncertainty quantification for sea state forecast

In this subsection, the procedure for quantification of sea state forecast uncertainty is described. It is assumed that forecast uncertainties of H_s and T_p are independent. Therefore, the conditional PDF of actual sea state with a given forecasted sea state can be expressed as Eq. (9).

$$f_{H_s^t T_p^t | H_s^f T_p^f}\left(h_s^t, t_p^t \middle| h_s^f, t_p^f\right) = f_{H_s^t | H_s^f}\left(h_s^t \middle| h_s^f\right) \cdot f_{T_p^t | T_p^f}\left(t_p^t \middle| t_p^f\right) \tag{9}$$

where $f_{H_s^t | H_s^f}(h_s^t | h_s^f)$ and $f_{T_p^t | T_p^f}(t_p^t | t_p^f)$ describe the probability that actual H_s and T_p may occur under given forecasted H_s and T_p, respectively. To establish these two conditional PDFs, the forecast error is first identified, and then the conditional PDF of the actual sea state is obtained by converting that of the forecast error. The forecast errors ε_h and ε_t used in this study are defined in Eqs. (10) and (11), which can reflect the percentage of forecast errors in H_s and T_p.

$$\varepsilon_h = \frac{H_s^t}{H_s^f} \tag{10}$$

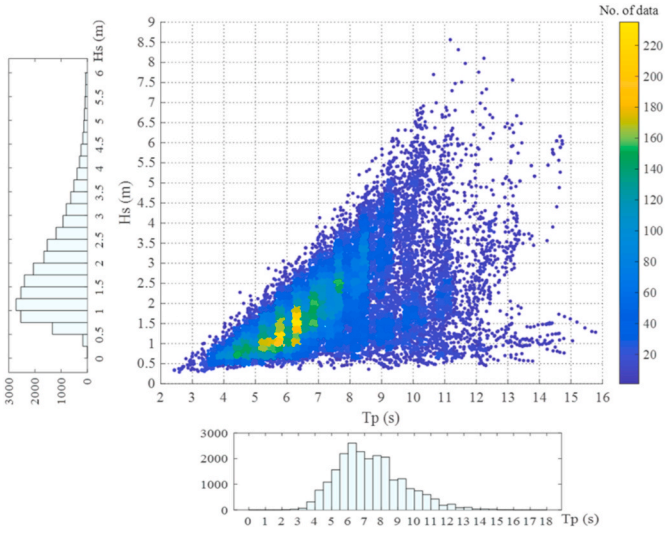

Fig. 2. Scatter plot of sea states at the North Sea center.

$$\varepsilon_t = \frac{T_p^t}{T_p^f} \tag{11}$$

Since marine operations are normally executed in relatively low sea states, it is reasonable to analyze the forecast error with respect to the range of H_s and T_p. For this purpose, forecasted data as well as corresponding forecast errors should be categorized. Sea states of the North Sea center (an offshore site at the central part of the North Sea, refer to the site 15 in Li et al. [39]) are taken as an example to illustrate this procedure. Fig. 2 shows a scatter plot of H_s and T_p as well as their respective histograms, based on the hindcast data of the CERA-20C dataset [40] by the ECMWF from 2001 to 2009. According to the displayed scatter plot, the interval of the H_s group is set to 0.5 m, and the group is named using the center value of the interval. For instance, the error group '1.5 m' represents forecasted significant wave height between 1.25 m and 1.75 m. In order to ensure that there are sufficient data to fit uncertainty distributions in all groups, all errors with H_s lower than 0.75 m and higher than 3.75 m are classified as '0.5 m' and '4 m' group respectively. Likewise, all T_p errors are categorized into different groups in terms of forecasted T_p with an interval of 1s. All errors of T_p lower than 5.5 s and higher than 9.5 s are classified as '5 s' group and '10 s', respectively. In addition, it is important to emphasize that the considered sea state range is site specific and should be determined according to the characteristics of the target sea areas.

Subsequently, error distribution for each group can be fitted. Both ε_h and ε_t are modelled as Gaussian distributed, whose parameters should be estimated separately based on errors in the group. Correspondingly, the conditional PDFs can be expressed as Eqs. (12) and (13) respectively.

$$f_{E_h|H_s^f}\left(\varepsilon_h \middle| h_s^f\right) = \frac{1}{\sqrt{2\pi}\sigma_{\varepsilon h}} exp\left[-\frac{1}{2}\left(\frac{\varepsilon_h - \mu_{\varepsilon h}}{\sigma_{\varepsilon h}}\right)^2\right] \tag{12}$$

$$f_{E_t|T_p^f}\left(\varepsilon_t \middle| t_p^f\right) = \frac{1}{\sqrt{2\pi}\sigma_{\varepsilon t}} exp\left[-\frac{1}{2}\left(\frac{\varepsilon_t - \mu_{\varepsilon t}}{\sigma_{\varepsilon t}}\right)^2\right] \tag{13}$$

where mean value $\mu_{\varepsilon h}$ and standard deviation $\sigma_{\varepsilon h}$ are functions of H_s^f and T_L. Mean value $\mu_{\varepsilon t}$ and standard deviation $\sigma_{\varepsilon t}$ are functions of T_p^f and T_L.

$$\mu_{\varepsilon h} = \mu_{\varepsilon h}\left(h_s^f,\ T_L\right) \tag{14}$$

$$\sigma_{\varepsilon h} = \sigma_{\varepsilon h}\left(h_s^f,\ T_L\right) \tag{15}$$

$$\mu_{\varepsilon t} = \mu_{\varepsilon t}\left(t_p^f,\ T_L\right) \tag{16}$$

$$\sigma_{\varepsilon t} = \sigma_{\varepsilon t}\left(t_p^f,\ T_L\right) \tag{17}$$

Based on the expressions of ε_h and ε_t, actual H_s and T_p are also Gaussian distributed and can be described as Eqs. (18) and (19). They reflect the forecast uncertainty in forecasted sea states.

$$h_s^t = \varepsilon_h \cdot h_s^f \sim\ N\left(h_s^f \cdot \mu_{\varepsilon h},\ h_s^{f^2} \cdot \sigma_{\varepsilon h}^2\right) \tag{18}$$

$$t_p^t = \varepsilon_t \cdot t_p^f \sim\ N\left(t_p^f \cdot \mu_{\varepsilon t},\ t_p^{f^2} \cdot \sigma_{\varepsilon t}^2\right) \tag{19}$$

3.4. Extreme response analysis for marine operations

In this section, the method for evaluating the conditional distribution of the extreme response for a given sea state will be briefly introduced. Normally, the extreme response distribution is built based on the dynamic responses by numerical analysis. According to the nature of the problem, two different methods are mainly applied, i.e. frequency domain (FD) and time domain (TD) methods. Regarding marine operations, for problems that can be considered under a linear assumption, it is possible to study the dynamic response in frequency domain to significantly reduce computational cost. Whereas for complex non-linear systems, time domain response analysis approach is more suitable.

3.4.1. Frequency domain analysis

When analyzing the dynamic response of an offshore structure subjected to wave loads in frequency domain, it is assumed that the response amplitude y_a varies linearly with the wave amplitude ζ_a for each frequency. Hence, the dynamic response can be analyzed in frequency domain. Specifically, the transfer function $h_{\xi Y}(\omega)$ is utilized to characterize the deterministic relation between wave process $\xi(t)$ and response process $Y(t)$, reflecting the effect of a given sea state on the marine structure. Correspondingly, the response spectrum $S_{YY}(\omega; h_s^t, t_p^t)$ can be given by

$$S_{YY}\left(\omega; h_s^t, t_p^t\right) = |h_{\xi Y}(\omega)|^2 \cdot S_{\xi\xi}\left(\omega; h_s^t, t_p^t\right) \tag{20}$$

where $S_{\xi\xi}(\omega; h_s^t, t_p^t)$ is the wave spectrum for a given sea state (h_s^t, t_p^t). $|h_{\xi Y}(\omega)|$ is the absolute value of transfer function.

Given that the wave surface process can be modelled as a Gaussian process, the response process can also be modelled as a Gaussian process due to the assumption of linearity. Correspondingly, it is reasonable to model the global response maxima R_o as a Rayleigh distribution under a given sea state, as shown in Eq. (21).

$$F_{R_o|H_s^t T_p^t}\left(r_0|h_s^t, t_p^t\right) = 1 - \exp\left[-\frac{1}{2}\left(\frac{r_0}{\sigma_Y\left(h_s^t, t_p^t\right)}\right)^2\right] \tag{21}$$

where $\sigma_Y^2(h_s^t, t_p^t)$ is the variance defined by Eq. (22), in which $m_{YY}^{(0)}(h_s^t, t_p^t)$ is the zero-th order spectral moment.

$$\sigma_Y^2\left(h_s^t, t_p^t\right) = m_{YY}^{(0)}\left(h_s^t, t_p^t\right) \tag{22}$$

The j-th order spectral moments $m_{YY}^{(j)}(h_s^t, t_p^t)$ can be defined as a general form

$$m_{YY}^{(j)}\left(h_s^t, t_p^t\right) = \int_0^\infty \omega^j S_{YY}\left(\omega; h_s^t, t_p^t\right) d\omega \tag{23}$$

Assume that all global response maxima of the given sea state are independent and identically distributed, the CDF of extreme response R can be given by Eq. (24), where n is the expected number of global maxima during the given period calculated by Eq. (25).

$$F_{R|H_s^t T_p^t}\left(r\middle|h_s^t, t_p^t\right) = \left\{1 - \exp\left[-\frac{1}{2}\left(\frac{r}{\sigma_Y\left(h_s^t, t_p^t\right)}\right)^2\right]\right\}^n \tag{24}$$

$$n = \frac{T_E}{T_{m02}} \tag{25}$$

where T_{m02} is the mean zero-up-crossing period, given by

$$T_{m02} = 2\pi\sqrt{\frac{m_{YY}^{(0)}}{m_{YY}^{(2)}}} \tag{26}$$

As n increases, this CDF can be reasonably approximated by the Gumbel distribution, which is shown in Eq. (27).

$$F_{R|H_s^t T_p^t}\left(r\middle|h_s^t, t_p^t\right) = \exp\left\{-exp\left[-\frac{r-\gamma}{\beta}\right]\right\} \tag{27}$$

where γ and β are the location and scale parameters expressed as

$$\gamma = \sigma_Y\left(h_s^t, t_p^t\right)\sqrt{2\ln n} \tag{28}$$

$$\beta = \frac{\sigma_Y\left(h_s^t, t_p^t\right)}{\sqrt{2\ln n}} \tag{29}$$

In summary, the procedure of estimating the extreme response distribution in frequency domain used in the response-based alpha-factor method is as follows:

1) For a given sea state, the corresponding wave spectrum $S_{\xi\xi}(\omega)$ can be generated. For instance, the wave condition can be described by a JONSWAP spectrum, that is the most commonly used wave spectrum in the North Sea area.
2) Meanwhile, for a specific offshore structure, the motion\force transfer functions in frequency domain can be obtained from hydrodynamic software (such as WAMIT [41] and HYDROD [42]) using potential panel theory.
3) Afterwards, the response spectrum $S_{YY}(\omega)$ is calculated by Eq. (20). All statistical information such as the variance $\sigma_Y^2(h_s^t, t_p^t)$ can be derived from it.
4) The Gumbel parameters can thereby be calculated based on Eqs. (28) and (29). Finally, the extreme response distribution under the given sea state $F_{R|H_s^t T_p^t}(r|h_s^t, t_p^t)$ is determined according to Eq. (27). Based on Eq. (27), the characteristic value of the dynamic response corresponding to a target exceedance probability can be calculated.

3.4.2. Time domain analysis

For marine operations like blade installation of offshore wind turbine, there exists a number of non-linear sources such as second-order wave forces on floating vessel, aerodynamic loads on blade and so on. Hence, dynamic response of the system should be addressed in time domain. In this case, the assumption of Rayleigh distributed global maxima is no longer valid. Nevertheless, a

Gumbel extreme value distribution is still valid for most cases [43], but the expressions of Gumbel parameters shown in Eqs. (28) and (29) need to be modified. To find Gumbel parameters, it is necessary to fit the extreme response distribution based on the response time series from the time domain simulation. The procedure is described as follows:

1) For a given sea state, perform the time domain simulation of the operation during the operational duration T_E (e.g. 10 min) and get a realization of the dynamic response. From the realization, the response maxima r can be extracted.
2) To better fit the tail of the extreme response distribution, it is necessary to perform multiple simulations under the same sea state to extract a sufficient number of maxima. Hence, repeat the simulation k times with random wave seeds. Then k independent response maxima $\{r_1, r_2, r_3, \ldots, r_k\}$ can be obtained.
3) According to the series of response maxima, the Gumbel distribution can be fitted by different methods, e.g., the method of moments, maximum likelihood estimation and so on. Based on the fitted Gumbel distribution, the related characteristic value can be calculated, corresponding to a target exceedance probability from the extreme response distribution.
4) Repeat the procedure for a large number of different sea states, the continuous functions of the Gumbel parameters can be obtained, which are the functions of H_s and T_p.

$$\gamma = \gamma\left(h_s^t, t_p^t\right) \tag{30}$$

$$\beta = \beta\left(h_s^t, t_p^t\right) \tag{31}$$

3.5. Derivation of the response-based alpha-factor

Followed by the weather forecast analysis and the extreme response analysis, the response-based alpha-factor α_R for a given sea state can be calculated by Eq. (32):

$$\alpha_R = \frac{R_E}{R_{E\_WF}} \tag{32}$$

where R_E is the characteristic value of the limiting response parameter within an operational duration T_E in a given sea state. It is defined as the extreme response with an exceedance probability (e.g., 10^{-4}) from the extreme value distribution. The definition of R_{E_WF} is similar to R_E but considering the forecast uncertainty of the sea state.

1) Calculation of R_E

When the weather forecast uncertainty is not considered, the forecasted sea state is regarded as the true value, i.e. (H_s^t, T_p^t). In this sea state, the extreme response distribution of a specific operation can be estimated directly by frequency- or time-domain response analysis approaches. The PDF of the structural extreme response is denoted as $f_{R|H_s^t T_p^t}(r' \,|\, h_s^t, t_p^t)$, and its CDF can be expressed as Eq. (33).

$$F_R(r) = \int_0^r f_{R|H_s^t T_p^t}\left(r' \,|\, h_s^t, t_p^t\right) dr' \tag{33}$$

By solving Eq. (34) with a certain exceedance probability (e.g., 10^{-4}), the R_E value under the sea state can be determined. It should be noted that the target exceedance probability depends on the type of operation and consequences of failure events.

$$1 - F_R(R_E) = 10^{-4} \tag{34}$$

For marine operations, the exceedance probability of the extreme response is normally set to 10^{-4}. However, the selection of such exceedance probability level is subjected to discussion. The target level can reflect the consequences of operation failure and one may also consider for example 10^{-2} for marine operations if the consequence of failure is not significant. For instance, for the mating operation by an installation vessel, the motion response of the crane tip can be regarded as a limiting response parameter. It is not a structural response parameter like lift wire tension. Large crane tip motion will lead to unsuccessful operation, but may not cause any structural failure or operation failure. Operator may try a second operation, if the first operation is not possible. Therefore, in this case, the characteristic values of the limiting parameter can be derived on the basis of extreme response analysis corresponding to a relatively high exceedance probability level.

2) Calculation of R_{E_WF}

When the weather forecast uncertainty is taken into account, the forecasted sea state cannot be regarded as the true value directly. Instead, for a forecasted sea state, there are many possibilities for the actual sea state. Therefore, it is of importance to establish the conditional PDF of actual sea state under a given forecasted sea state, i.e. $f_{H_s^t T_p^t | H_s^f T_p^f}(h_s^t, t_p^t \,|\, h_s^f, t_p^f)$. In this case, the value of R_{E_WF} can be determined by a joint PDF of the extreme response R and the actual sea state (H_s^t, T_p^t), that is established as

$$f_{RH_s^tT_p^t}\left(r^{'},h_s^t,t_p^t\right)=f_{R\left|H_s^tT_p^t\right.}\left(r^{'}\left|h_s^t,t_p^t\right.\right)\cdot f_{H_s^tT_p^t\left|H_s^fT_p^f\right.}\left(h_s^t,t_p^t\left|h_s^f,t_p^f\right.\right) \tag{35}$$

where $f_{R|H_s^tT_p^t}(r^{'}|h_s^t,t_p^t)$ is the conditional PDF of the extreme response with a given actual sea state. $f_{H_s^tT_p^t|H_s^fT_p^f}(h_s^t,t_p^t|h_s^f,t_p^f)$ reflects the forecast uncertainty, which accounts for the uncertainty in both H_s and T_p forecasts.

Through integration, the marginal CDF of R can be obtained, as shown in Eq. (36).

$$F_R^{WF}(r)=\int_0^r\int_0^{+\infty}\int_0^{+\infty}f_{R\left|H_s^tT_p^t\right.}\left(r^{'}\left|h_s^t,t_p^t\right.\right)\cdot f_{H_s^tT_p^t\left|H_s^fT_p^f\right.}\left(h_s^t,t_p^t\left|h_s^f,t_p^f\right.\right)dh_s^tdt_p^tdr^{'} \tag{36}$$

By solving Eq. (37), the corresponding R_{E_WF} value with the same exceedance probability as R_E can be determined.

$$1-F_R^{WF}(R_{E\_WF})=10^{-4} \tag{37}$$

3) Calculation of α_R

For the given sea state, by substituting R_E and R_{E_WF}, the corresponding α_R value can be calculated by Eq. (32). α_R depends on the type and duration of the marine operation, the forecast variable, the lead time, etc., mentioned in Section 3.1. For a specific marine operation, repeating this procedure in different sea states, the tabulated response-based alpha-factor α_R can be obtained.

3.6. Application of the response-based alpha-factor

According to the α-factor proposed by DNV, the allowable sea states in terms of H_s can be adjusted directly by the selected α. In comparison, the α_R proposed in this study is from the perspective of response, and it also depends on the type of operations. Besides, α_R takes into account the forecast uncertainty in both H_s and T_p. Correspondingly, it should be more comprehensive and reliable in the application of marine operations. However, the α_R is a response-based criterion and cannot be used directly to correct sea state limits. In this case, allowable sea states have to be re-assessed considering explicitly the forecast uncertainty and depending on the forecast horizon. The procedures of applying the α_R in marine operations are summarized as follows:

- When sea state forecasts are available, based on the aforementioned procedure, forecast uncertainty analysis can be carried out and characteristic values R_{E_WF} for various sea state scenarios can be obtained for a specific operation, in terms of the forecast lead time. For a certain lead time, different sea states under which R_{E_WF} equals to the allowable limit of response can be found. These sea states consist of a contour line representing the maximum sea states that the operation can be safely executed. Following this procedure, one can generate contour lines for different forecast lead times. In the execution phase, when sea state forecasts are provided, they can be compared with corresponding contour lines with the same forecast lead time. The comparison result could support decision-making of the operation.
- In addition, the tabulated α_R factors can be directly used to correct R_E values without performing forecast uncertainty analysis of sea states. For a specific operation, characteristic values R_E of the limiting parameter can be calculated for different sea states. These R_E values can be adjusted by pre-calculated α_R factors under same sea states to account for the weather forecast uncertainty. And therefore, R_{E_WF} values for the operation can be obtained. Likewise, by comparing the R_{E_WF} with the allowable limit, the allowable sea states involving weather forecast uncertainty can be assessed. In the subsequent execution phase, the allowable sea states can be compared with the weather forecasts to find workable weather windows.

These will be further discussed in Section 4.5.

4. Case study on single blade installation of offshore wind turbines

In this section, the proposed method is applied to the blade installation of offshore wind turbine by a semi-submersible crane vessel, in order to illustrate its application. Compared with jack-up crane vessels, installation by floating crane vessels is more challenging. This is mainly because floating crane vessels are more sensitive to wave conditions. The wave-induced motion of the floating crane vessel will contribute to a significant motion at the crane tip. The crane tip motion could further increase the motion of the blade to some extent and challenge the security of the offshore wind turbine installation. Thus, the uncertainty inherent in sea state forecasts should be dealt with and it is of great importance to investigate their effect on the offshore blade installation. In this case study, only the crane tip motion is focused on. Given that the wave-induced vessel motion is the main source of the crane tip motion, the wave condition is of main interest and the wind condition is not considered in this paper.

4.1. Study area and forecasting methods

The North Sea center is focused in this study, since various marine operations related to the offshore wind turbine installation have been studied within this area [4,44–48]. At the target site, short-term wave conditions, characterized by H_s and T_p of the total sea, are

forecasted based on machine learning algorithms. Two related methods, i.e., the time series-based machine learning (TSML) method and the physics-based machine learning (PBML) method, are adopted for one-day-ahead wave forecasting. The former one is a pure machine learning method, and Wu et al. [49] have compared different TSML methods for multi-step-ahead forecasting of wave and wind conditions. Among them, the ANN M − 1 model with univariate input variable is utilized in this paper due to the high computational efficiency. Specifically, the artificial neural network (ANN) is employed as the machine learning algorithm for forecasting. To generate multi-step-ahead forecasts, a multi-step-ahead forecast strategy, that is the M − 1 model is applied, which uses the relationship between last M data up to the current time and the next data to build the model, and then makes forecast recursively. Besides, 'univariate input variable' refers to that the future data of a weather variable (e.g., H_s) is forecasted only based on its past data. The ANN M − 1 model for H_s and T_p forecasting can be expressed as Eqs. (38) and (39) respectively. A preliminary study on the structure of models with different M values indicates that the model with M equal to 5 has better performance and can be used for the TSML model. For detailed description of the TSML model and parameters, as well as discussions on the multi-step-ahead forecast results at the North Sea center, refer to Wu et al. [29,49].

$$H_s(t+1) = f_h^T\left(H_s(t), H_s(t-1), \ldots, H_s(t-M+1)\right) \tag{38}$$

$$T_p(t+1) = f_t^T\left(T_p(t), T_p(t-1), \ldots, T_p(t-M+1)\right) \tag{39}$$

where t is the current time. f_h^T and f_t^T are TSML models of H_s and T_p, respectively.

In addition to the TSML method purely relying on the wave time series, the PBML method which combines physical phenomenon of wave evolution and machine learning algorithm, is utilized as another forecasting method in the study. This model depicts a dynamic system, in which two important parts are required as the input to forecast sea states, namely the initial condition and the forcing. Specifically, the model is initialized with the wave condition characterized by significant wave height H_s and peak wave period T_p at the current time t. Besides, wind conditions are regarded as the forcing source, which is consistent with the considerations in the physics-based numerical wave models like WAM [12] and SWAN [13]. In the PBML model, the wind forcing at two continuous time steps up to the forecast step $t + N$ are applied to reflect the dynamic characteristics of wind field, while other processes like wave dissipation and redistribution are automatically learned by machine learning algorithms from data. The corresponding forecasting models of H_s and T_p based on the PBML method are expressed in Eqs. (40) and (41) respectively. It should be noted that the PBML method can be utilized for both small domain and a single location. In this study, a small domain containing 9 grid points is considered

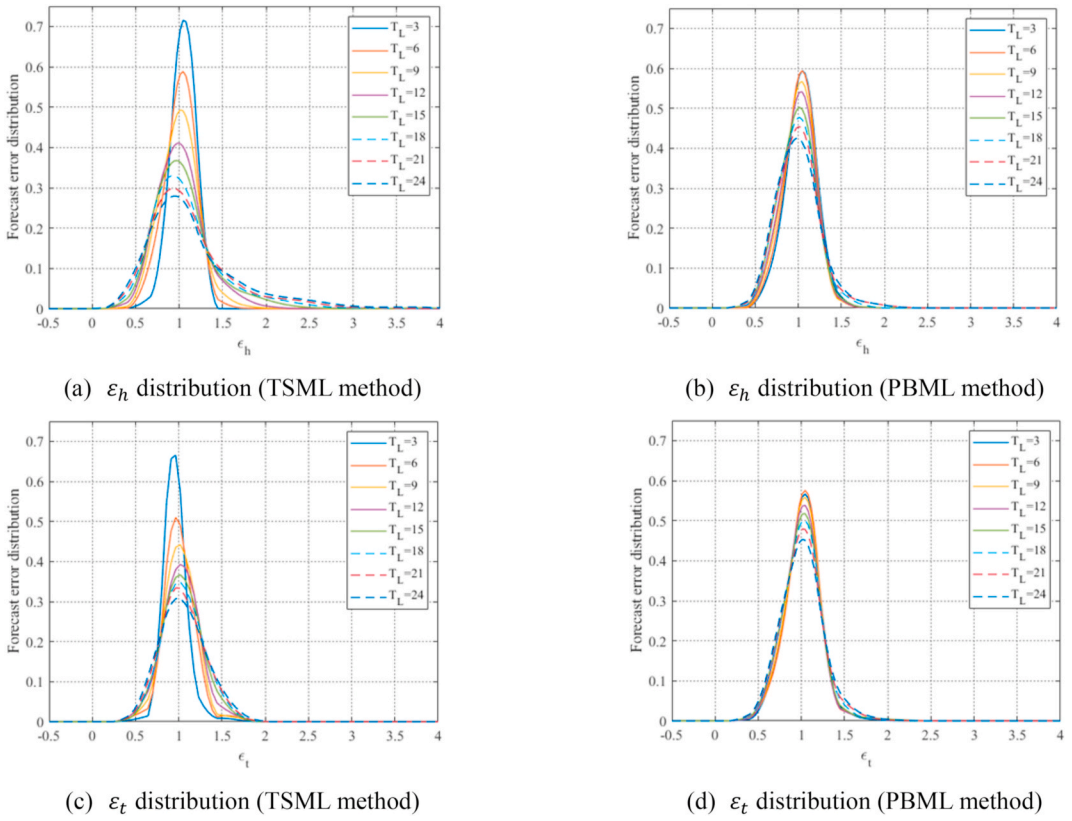

(a) ε_h distribution (TSML method) (b) ε_h distribution (PBML method)

(c) ε_t distribution (TSML method) (d) ε_t distribution (PBML method)

Fig. 3. Forecast error PDFs of H_s and T_p at different lead times $_{(a)}$ ε_h distribution (TSML method) $_{(b)}$ ε_h distribution (PBML method) $_{(c)}$ ε_t distribution (TSML method) $_{(d)}$ ε_t distribution (PBML method).

and the forecast accuracy of the center point is analyzed. For details about the model description and its forecast performance at the North Sea center, refer to Wu et al. [33].

$$H_s(t+N) = f_h^P\left(H_s(t), T_p(t), U_w(t+N), U_w(t+N-1), D_u(t+N), D_u(t+N-1)\right) \tag{40}$$

$$T_p(t+N) = f_t^P\left(H_s(t), T_p(t), U_w(t+N), U_w(t+N-1), D_u(t+N), D_u(t+N-1)\right) \tag{41}$$

where N is the forecast step. f_h^P and f_t^P are PBML models of H_s and T_p. D_u and U_w are the wave direction and mean wind speed, respectively.

To establish above forecasting models, it is ideal to use long-term historical measurement data. However, due to the limited amount of measurement data and the high quality of the hindcast data, the hindcast data are utilized in the study. Hindcast wave and wind data are from the CERA-20C dataset [40] within the period from 2001 to 2010 at the North Sea center. The whole dataset is divided into two parts: the data of the first nine years (2001–2009) are the training data used for model establishment and validation, and the data of the last year (2010) are the testing data used for forecast uncertainty quantification. Noted that the temporal resolution of the CERA-20C data is 3 h. Hence, in order to perform one-day-ahead forecasts, eight iterations are required for the TSML model, and N needs to be selected from one to eight for the PBML model. In addition, it should be emphasized that in this paper, only forecasts of the total sea are considered and utilized for the following uncertainty quantification analysis. For the swell and wind sea, they were forecasted separately in Ref. [33], in which the corresponding uncertainty models are built. However, the effect of their forecast uncertainties on marine operations are not addressed in the paper.

4.2. Forecast results, uncertainty quantification and trend analysis

Based on the trained forecasting models, one-day-ahead H_s and T_p forecasts can be produced. Following the method described in Section 3.3, distributions of the forecast error ε_h and ε_t (defined in Eqs. (10) and (11)) can then be generated. The PDFs of the ε_h and ε_t for different lead times are plotted in Fig. 3, from which two conclusions can be drawn. On one hand, the error seems to follow the Gaussian distribution, and this observation is directly used in the following study without further verification. On the other hand, the distributions show more discrepancies as the lead time increases. This phenomenon illustrates that forecast uncertainty would increase as the increase of the forecast horizon. By comparison, it seems that when the lead time less than 6 h, the TSML method has better forecast performance, while the advantage of the PBML method is more obvious as the lead time further increases.

As aforementioned, forecast errors should be analyzed with respect to the range of H_s and T_p. Figs. 4–7 present statistics of ε_h and ε_t (discrete points in different colors), which are functions of lead time T_L for different error groups by the TSML and PBML methods, respectively. It is evident that error statistics show certain fluctuations, caused by the statistical uncertainty due to the limited number of forecasts. This phenomenon can be observed especially in the cases with small significant wave height and short wave period. This is because for the definition of the forecast error, small values will have larger error ratio than the large values for the same absolute error, even if the discrepancy between the forecast and actual are the same. To eliminate these effects to a certain extent, the trend analysis is performed subsequently. The trend lines (linear) of the discrete points in the above figures are estimated using the least-square fit algorithm and they are shown as the solid lines in the corresponding figures. From the generated trend lines, one can observe that both $\mu_{\varepsilon h}$ and $\mu_{\varepsilon t}$ are close to one in different groups, except for cases with H_s in the range of 0.5–1.0 m by the TSML method. Meanwhile, the level of $\sigma_{\varepsilon h}$ and $\sigma_{\varepsilon t}$ increase as the lead time T_L increases and the range decreases. By using error statistics along trend lines, the PDF of actual sea states considering uncertainties can be generated, referring to Eqs. (18) and (19).

4.3. Motion response analysis of the crane tip

Crane tip motion during the final mating phase of blade installation can be analyzed by applying frequency domain or time domain method. Since the crane tip motion is mainly caused by the semi-submersible's wave-induced motion and dynamic properties of the system do not significantly change in time, frequency-domain response analysis approach is a reasonable choice for the advantage of

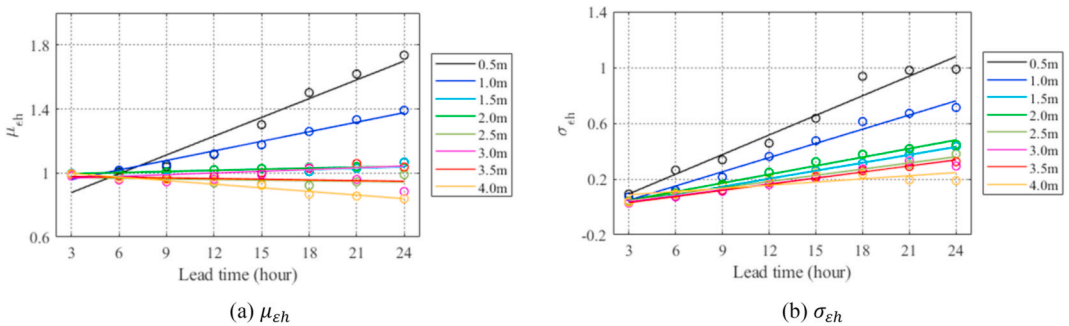

(a) $\mu_{\varepsilon h}$ (b) $\sigma_{\varepsilon h}$

Fig. 4. Statistics of ε_h and trend line analysis for different lead times (TSML method) (a) $\mu_{\varepsilon h}$ (b).$\sigma_{\varepsilon h}$

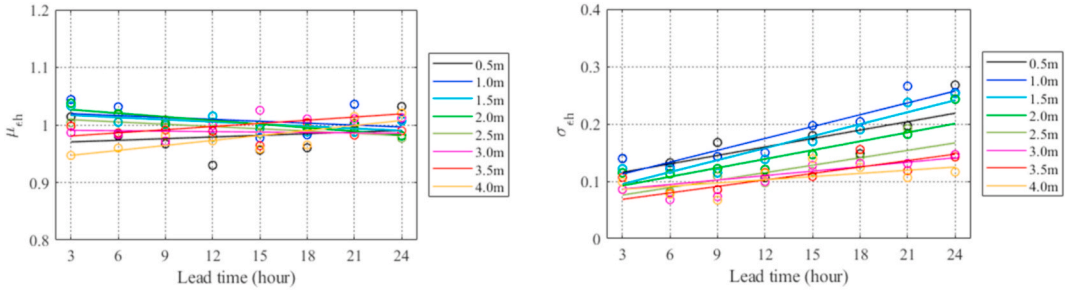

(a) $\mu_{\varepsilon h}$ (b) $\sigma_{\varepsilon h}$

Fig. 5. Statistics of ε_h and trend line analysis for different lead times (PBML method) (a) $\mu_{\varepsilon h}$ (b).$\sigma_{\varepsilon h}$

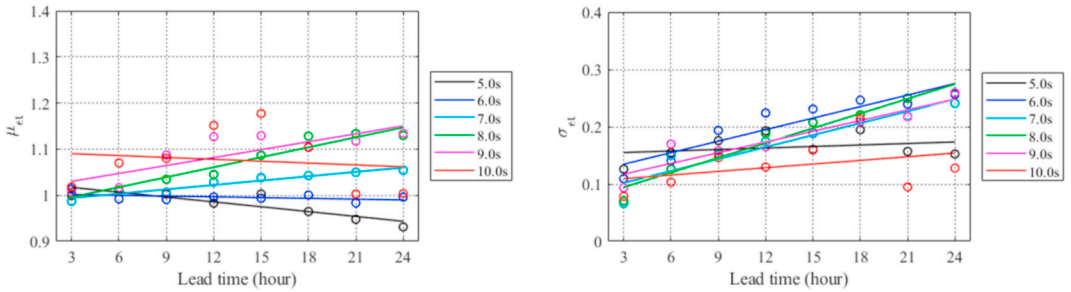

(a) $\mu_{\varepsilon t}$ (b) $\sigma_{\varepsilon t}$

Fig. 6. Statistics of ε_t and trend line analysis for different lead times (TSML method) (a) $\mu_{\varepsilon t}$ (b).$\sigma_{\varepsilon t}$

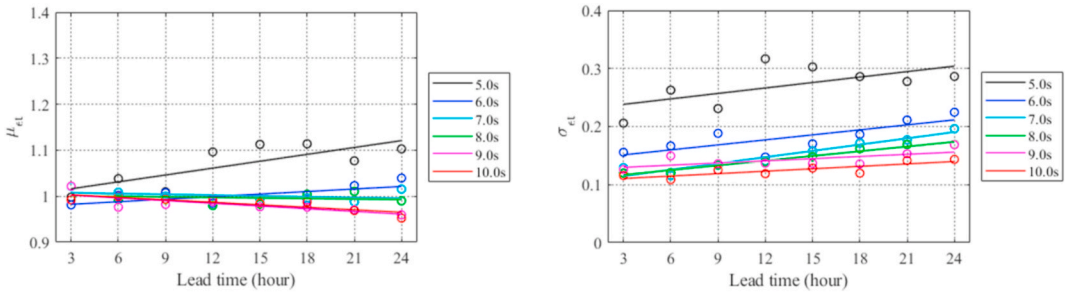

(a) $\mu_{\varepsilon t}$ (b) $\sigma_{\varepsilon t}$

Fig. 7. Statistics of ε_t and trend line analysis for different lead times (PBML method) (a) $\mu_{\varepsilon t}$ (b).$\sigma_{\varepsilon t}$

the high cost efficiency. A preliminary study on dynamic response analysis of the crane tip motion in frequency- and time-domain indicates that there is a good agreement of the crane tip motion between two methods. Thus, the frequency-domain approach using spectral analyses is considered for the response calculation of the crane tip in this study.

4.3.1. Numerical modeling

Based on the frequency-domain response analysis approach, the motion of semi-submersible and crane tip can be directly obtained by the motion transfer functions and wave spectra. The first-order motion transfer functions for the semi-submersible are obtained

Table 1
Main properties of the installation system.

Parameters		Unit	Values
Semi-submersible	Length	M	175
	Breadth	M	87
	Operational draught	M	26.1
Crane tip position in the vessel-related coordinate system		M	(66, 65.3, 144.9)

from the published hydrodynamic code HydroD, using potential panel theory. Based on the motion transfer functions of the semi-submersible and the relative coordinate of the crane tip to semi-submersible's COG, the motion transfer functions for the crane tip can be calculated. The dimensions of the semi-submersible and the relative coordinate of the crane tip are presented in Table 1. More detailed description of the model properties, refer to Zhao et al. [44]. The numerical model is illustrated in Fig. 8. In the figure, two right-handed coordinate systems, i.e., a vessel-related coordinate system O_v-$X_vY_vZ_v$ and a crane-related coordinate system O_c-$X_cY_cZ_c$, are used, whose origins are located at the center of the waterplane of the semi-submersible at rest and the crane tip, respectively. In this study, the beam sea condition is considered, which means that the incident wave angle θ_{wv} is zero. Besides, the simulation time is 10 min, which is consistent with the duration of the final mating phase of the blade installation.

In the beam sea condition, the transfer functions of the first-order motion of the semi-submersible are shown in Fig. 9. As expected, heave and roll motions of the semi-submersible are high. However, the pitch motion is also high in the beam sea. This is because in the numerical model, the pontoons of the semi-submersible are symmetric, while the columns are asymmetric in the *YOZ*-plane. This causes the vertical force on the pontoons on the left part of the floater with respect to the *YOZ* plane to be different from the vertical force on the right part. As a result, a moment is created along the *Y* axis, inducing the pitch motion of the semi-submersible. Besides, the natural periods of the semi-submersible in heave, roll and pitch are presented in Table 2. As displayed, the natural periods in heave, roll and pitch are between 18 s and 24 s. Multiple peaks in heave and pitch can be observed in Fig. 9, indicating that there is a strong coupling between heave and pitch for the semi-submersible. Based on the motion transfer functions of the semi-submersible, the transfer functions of the first-order motion of the crane tip in 3 degree-of-freedoms (DOFs) are calculated, as shown in Fig. 10.

Although the transfer functions of the semi-submersible for the roll and pitch resonance periods are high, they will not affect the results since the frequency-domain method is used and the relevant wave periods for wind turbine installation are very small. In the paper, the main focus of T_p is in the range of 5–10 s. Correspondingly, it is only related to the transfer functions with a frequency of 0.6–2.5 rad/s. An example of the wave spectrum and the resulting motion spectra of the crane tip is illustrated in Fig. 11. In the figure, the sea state is described by a JONSWAP spectrum with a peakedness factor γ of 3.3 [50], $H_s = 2$ m and different T_p (from 5 s to 10 s), and the corresponding motion spectra are established by spectral analysis.

As illustrated in Fig. 11, for a given H_s, the shape of power spectra of crane tip motion is significantly affected by the selection of T_p. The spectrum peaks increase with increasing T_p values, which indicates that the crane tip motion is larger at sea state with larger T_p. This is because the relevant wave periods are well smaller than the natural periods of the semi-submersible roll (or pitch) motions and when the wave period increases, the roll (or pitch) motion increases. Moreover, characteristic values of the corresponding crane tip motion for 10^{-4} exceedance probability are calculated and presented in Fig. 12. The comparison among cases further proves the importance of T_p to crane tip motion. By comparing the crane tip motion in X_c, Y_c and Z_c directions in the crane-related coordinate system, it is visible that the motion in Y_c direction is larger than that in other two directions in the beam sea condition. Hence, only Y_c direction is concerned, and the crane tip motion refers to its motion in Y_c direction in the following analysis.

4.3.2. Extreme response analysis in frequency domain

In frequency domain, the motion spectra of the crane tip can give a complete description of its statistical properties, and a Gumbel distribution can be adopted to describe the extreme crane tip motion. Thus, the characteristic value of the crane tip motion under certain exceedance probability can be identified from the simulation in FD, following the method described in Section 3.4.1. Fig. 13 gives an example of extreme response distributions with and without including weather forecast uncertainty. In this example, the characteristic value of crane tip motion (in Y_c direction in the crane-related coordinate system) is the extreme value in 10 min with an

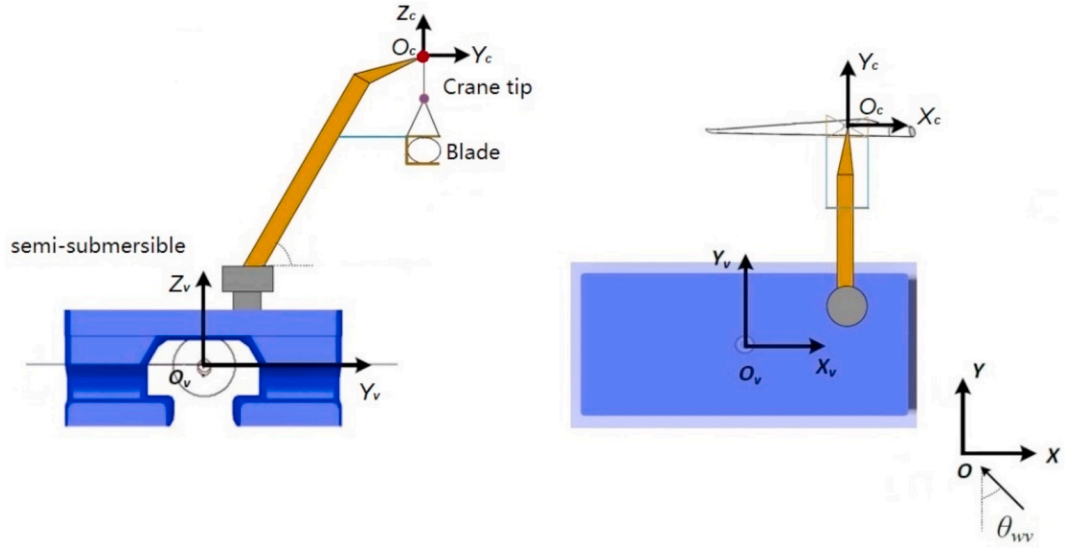

Fig. 8. Numerical model of the blade installation.

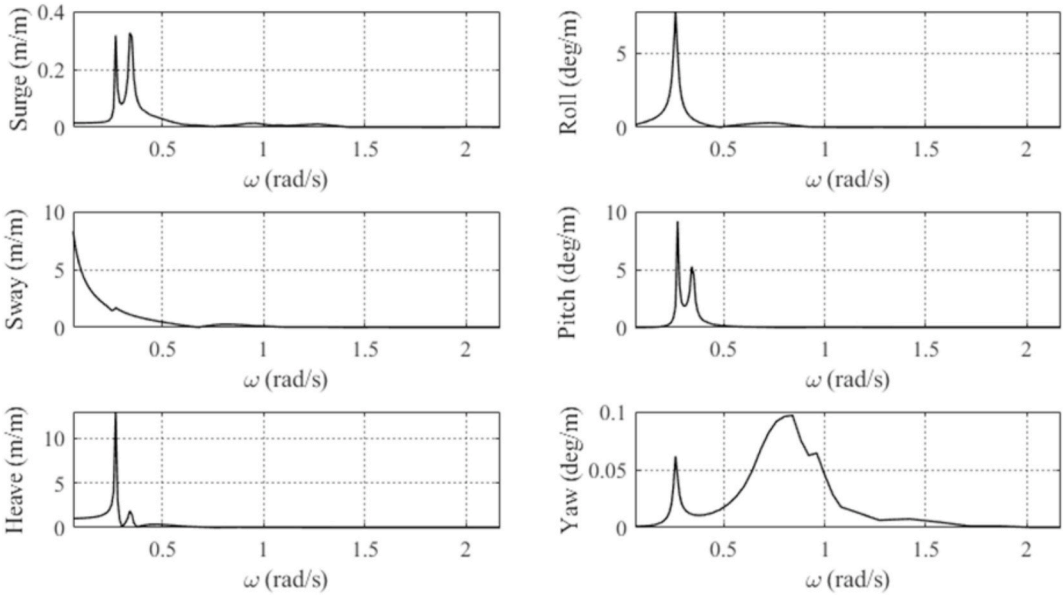

Fig. 9. Motion transfer functions of the semi-submersible in the beam condition (in the vessel-related coordinated system).

Table 2
The natural periods (s) of the semi-submersible's motions.

Vessel	Heave	Pitch	Roll
Semi-submersible	23.4	18.5	23.3

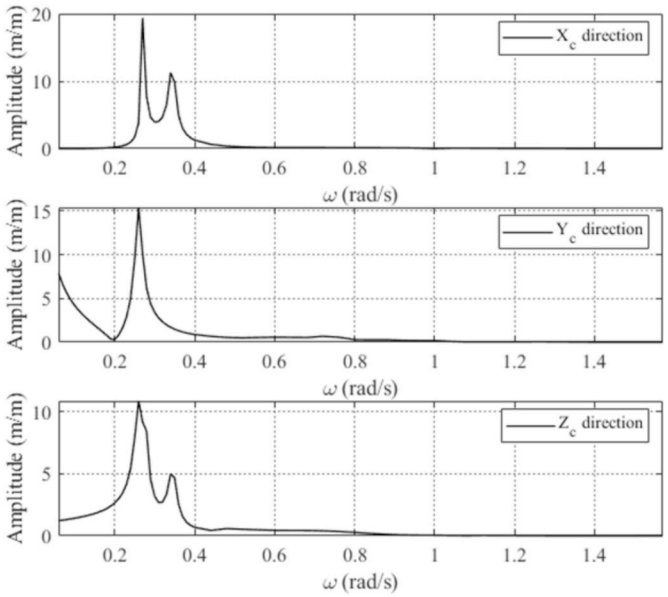

Fig. 10. Motion transfer functions of the crane tip in the beam condition (in the crane-related coordinated system).

exceedance probability of 10^{-4}. The TSML method is used in the sea state forecasting and T_L is 3 h.

The obvious difference between blue and black lines in Fig. 13 indicates that the uncertainty of sea state forecasts strongly affects the extreme value distribution. Since the weather forecast uncertainty is included, the blue distribution is much more dispersed than the black one. Based on these two distributions, characteristic values corresponding to an exceedance probability of 10^{-4} are selected respectively. By dividing them, the relevant response-based alpha-factor for the crane tip motion can be established.

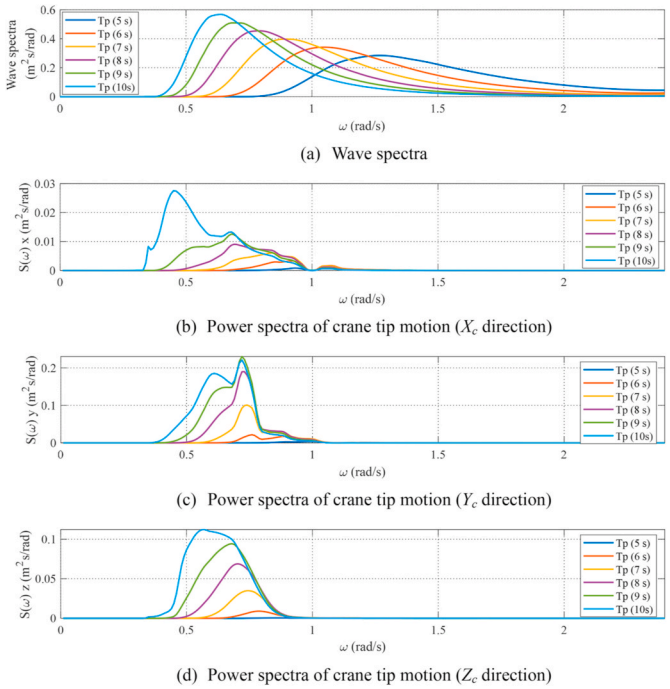

Fig. 11. Wave spectra and power spectra of crane tip motion for different T_p ($H_s = 2$ m) (a) Wave spectra (b) Power spectra of crane tip motion (X_c direction) (c) Power spectra of crane tip motion (Y_c direction) (d) Power spectra of crane tip motion (Z_c direction).

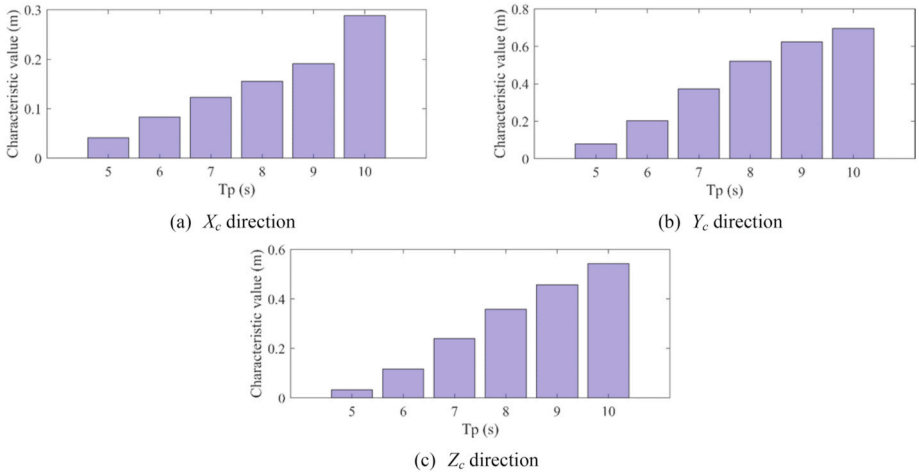

Fig. 12. Characteristic values of crane tip motion for different T_p ($H_s = 2$ m) *(a)* X_c direction *(b)* Y_c direction *(c)* Z_c direction.

Generally, the characteristic value is determined from the extreme value distribution with a target exceedance probability, to ensure the safety of the design with an acceptable low probability of damage or collapse. The target exceedance probability depends on the type of operation, the consequence of failure, etc. During the blade installation, since large crane tip motion may not lead to the installation operation failure, a larger probability of exceedance (i.e., 10^{-2}) can also be considered as well as 10^{-4} recommended in DNV standard. Fig. 14 shows the relevant results with the 10^{-2} exceedance probability under the same condition as shown in Fig. 13.

Following the same procedure, R_E and R_{E_WF} values regarding the crane tip motion with exceedance probabilities of 10^{-4} and 10^{-2} in different sea states can be estimated. Results with 10^{-4} exceedance probability are presented in Tables 3 and 4. The R_{E_WF} values still correspond to the TSML method with T_L of 3 h.

By comparison of results in Tables 3 and 4, it is visible that the R_{E_WF} values are generally larger than the corresponding R_E values when forecast uncertainties in sea states are involved. The degree of this difference reflects the effect of weather forecast uncertainty on the motion response. Based on R_E and R_{E_WF} values, corresponding α_R factors can be calculated. This will be summarized and analyzed in Section 4.4. Furthermore, characteristic values at other lead times can be calculated by the same procedure. Similar analysis can also

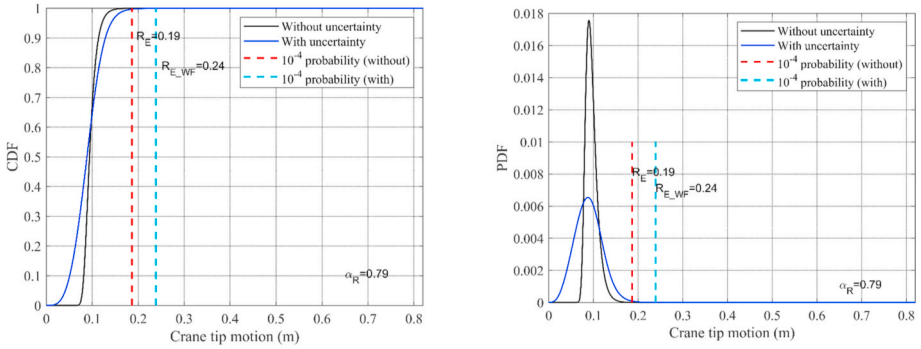

(a) CDF (b) PDF

Fig. 13. Extreme response distributions with and without considering weather forecast uncertainty (Example: $H_s = 1$ m, $T_p = 7$ s, TSML method, 10^{-4} exceedance probability) (a) CDF (b) PDF.

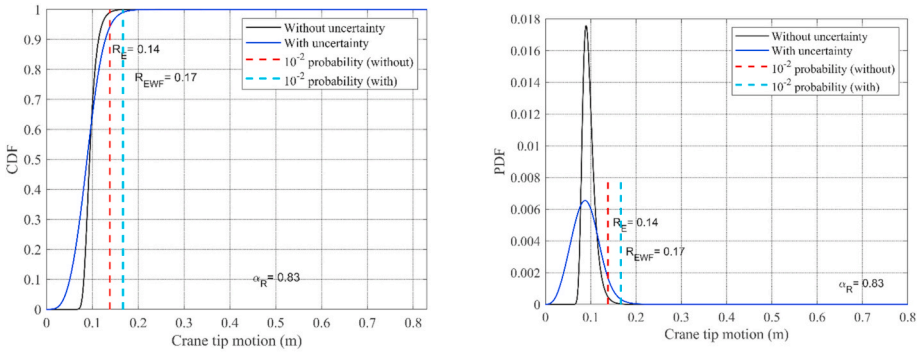

(a) CDF (b) PDF

Fig. 14. Extreme response distributions with and without considering weather forecast uncertainty (Example: $H_s = 1$ m, $T_p = 7$ s, TSML method, 10^{-2} exceedance probability) (a) CDF (b) PDF.

be performed with respect to the forecasts by the PBML method.

4.4. Response-based alpha-factor

For the definition of the response-based alpha-factor, an α_R of 1.0 presents the sea state forecast is completely correct. The farther it is from one, the greater the uncertainty implicit in the weather forecasts. Figs. 15 and 16 show α_R factors for the crane tip motion with exceedance probability of 10^{-4}. They use weather forecasts generated by the TSML and PBML methods, respectively. To investigate the effect of T_p forecast uncertainty on α_R, the variations of α_R with H_s in different T_p groups are plotted and displayed by solid lines with different colors. Besides, subfigures (a) and (b) in each figure show α_R at the lead time of 3 h and 24 h respectively, to explore the influence of the forecast horizon.

In addition to the α_R, the α-factors, extracted from the DNV standard [3], are plotted in figures for comparison. They correspond to the weather forecast Level C and are based on the work performed in JIP [30] during the years 2005–2007. According to the forecast

Table 3
R_E values (m) of the crane tip motion (10^{-4} exceedance probability).

H_s (m)	T_p (s)					
	5	6	7	8	9	10
0.5	0.02	0.05	0.10	0.13	0.16	0.17
1.0	0.04	0.10	0.19	0.26	0.31	0.35
1.5	0.06	0.15	0.28	0.40	0.47	0.52
2.0	0.08	0.20	0.37	0.52	0.62	0.70
2.5	0.10	0.26	0.47	0.65	0.78	0.87
3.0	0.12	0.31	0.56	0.78	0.94	1.04
3.5	0.14	0.36	0.65	0.91	1.09	1.22
4.0	0.16	0.41	0.75	1.04	1.25	1.39

Table 4
R_{E_WF} values (m) of the crane tip motion (T_L = 3 h, TSML method, 10^{-4}).

H_s (m)	T_p (s)					
	5	6	7	8	9	10
0.5	0.07	0.10	0.11	0.14	0.18	0.33
1.0	0.15	0.20	0.24	0.28	0.38	0.70
1.5	0.23	0.31	0.36	0.43	0.57	1.05
2.0	0.31	0.42	0.49	0.59	0.78	1.42
2.5	0.38	0.51	0.60	0.72	0.96	1.69
3.0	0.46	0.61	0.72	0.85	1.14	1.94
3.5	0.54	0.72	0.84	1.00	1.34	2.19
4.0	0.64	0.87	1.02	1.22	1.61	2.43

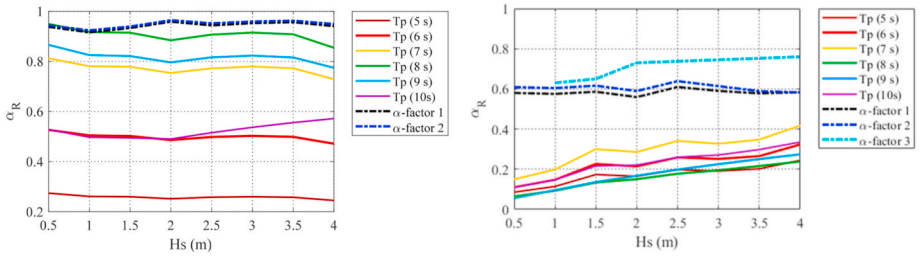

(a) Lead time T_L: 3 hours (b) Lead time T_L: 24 hours

Fig. 15. α_R vs. H_s in different T_p groups (TSML method) (a) Lead time T_L: 3 h (b) Lead time T_L: 24 h.

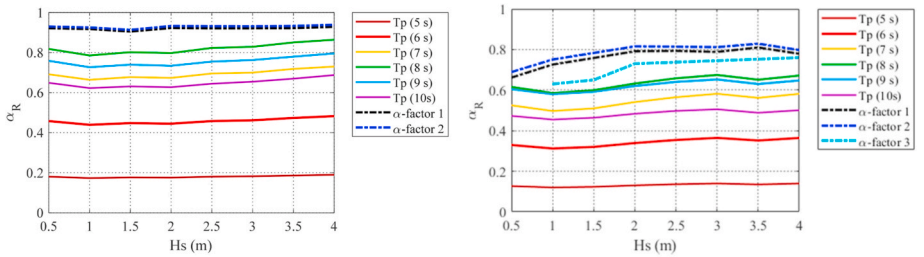

(c) Lead time T_L: 3 hours (d) Lead time T_L: 24 hours

Fig. 16. α_R vs. H_s in different T_p groups (PBML method) (c) Lead time T_L: 3 h (d) Lead time T_L: 24 h.

horizon of the α-factors in the DNV standard, only results with the lead time of 24 h are plotted in subfigures (b). Meanwhile, following the derivation process, α-factors are also calculated using the generated weather forecasts by TSML or PBML method, and are plotted in the corresponding figures. It should be noted that regarding the α-factor, $H_{\max}$ and $H_{\max\_WF}$ are estimated from the extreme wave height distributions during a given sea state reference period, that is 3 h in the study. This implies that the difference between the sea state reference period T_R and the operation duration T_E is not taken into account. For the sake of consistency, the α-factor generated by analyzing maximum wave heights during 10 min (i.e., the duration corresponds to the blade installation) is calculated and displayed as well. The properties of the considered correction factors are summarized in Table 5.

The response-based alpha-factor is a complex indicator and both the extreme response of offshore structures and weather forecast uncertainty affect its value. According to the above extreme response analysis, the characteristic response of the crane tip motion increases significantly with increasing H_s and T_p. However, this effect may not be equivalently reflected in the value of α_R. Fundamentally, this is due to the fact that the α_R is a ratio of the extreme responses without and with the consideration of the weather forecast uncertainty for a given sea state. In view of a frequency-domain approach is applied for motion analysis, the response of the system is very likely linear with respect to wave height. As a result, α_R does not change very much with H_s for a given T_p, as shown in Figs. 15 and 16. By contrast, the α_R varies greatly among different T_p groups. Nevertheless, the dependency of the α_R on T_p is not necessary to be the same as that of the characteristic responses on T_p. As can be observed in Fig. 12, for a given H_s, the characteristic response increases as T_p increases, while the α_R does not. The greatly contribution of the forecast uncertainty in T_p to the α_R might be the reason. For instance, as illustrated in Fig. 7, the forecast uncertainty in the T_p groups with 5–6 s is higher than that in other groups. This causes a large difference between R_E and R_{E_WF}, and therefore making the α_R lower in these two groups, as shown in Fig. 16.

In general, a large difference in α_R factors is observed in different T_p groups with the same H_s, indicating that T_p is not a negligible variable in the blade installation design using a floating crane vessel. However, uncertainty in T_p forecasts is not reflected in the widely

Table 5
Properties of the calculated factors.

Factor	Forecast uncertainty in H_s	Forecast uncertainty in T_p	The effect of weather forecast uncertainty on dynamic response	Reference period to estimate the characteristic value	Forecasting methods
α_R	✓	✓	✓	10 min	TSML or PBML
α-factor 1	✓			3 h	TSML or PBML
α-factor 2	✓			10 min	TSML or PBML
α-factor 3	✓			3 h	DNV standard

used α-factor. For instance, for the H_s group of 0.5 m in Fig. 15 (a), the α-factor 1 and α-factor 2 are 0.938 and 0.944 respectively, which are independent of T_p. By comparison, α_R varies from 0.27 to 0.95 considering forecast uncertainty of T_p in different T_p groups. Furthermore, the α-factor is purely generated by analyzing weather data while their effect on the dynamic response is not be considered. Comparison between subfigures (a) and (b) in the above two figures shows that although the α-factor decreases with the forecast horizon, the influence of the weather forecast uncertainty on the crane tip motion cannot be clearly identified, especially when the forecast horizon is long. This may because the dynamic response is not totally proportional to H_s, and T_p is essential for operations based on floating structures. Therefore, uncertainty in T_p forecasts should also be taken into account. Regarding the α_R, it can reflect the impact of sea state forecast uncertainties on the dynamic response and a large lead time induce a smaller correction factor. However, it should be emphasized that the α_R in this paper is generated for the installation system using a semi-submersible crane vessel with larger natural periods. Given that the α_R is an operation specific factor, it should be recalculated when other types of installation vessels (e.g., jack-up vessel or mono-hull vessel) are used. In those cases, its variations under various sea state forecasts may be different. In addition, the quality of weather forecasts is important to generate both the α-factor and the α_R. Compared to the PBML method, the TSML forecasting method makes the α_R decrease more when the lead time is extended to 24 h. The comparison results related to the three α-factors can also implicitly reflect the forecast performance of machine learning-based methods and physics-based numerical methods to a certain extent. However, it needs to be emphasized that this is not a strict comparison, because the conditions for generating the three α-factors are not exactly the same.

4.5. Allowable sea states in terms of crane tip motion

Regarding the allowable sea states assessment, H_s-based alpha-factor derived by DNV can be used directly as a correction factor that is multiplied with the actual H_s limit of marine operations for decision-making when weather forecast uncertainty is considered. This is done by comparing the forecasted H_s with the new H_s limit with the alpha-factor. However, the response-based alpha-factor derived above cannot be directly used in combination with the forecasted values of H_s and T_p for decision-making of marine operations. This is because it is defined as a correction factor based on the response parameter, not on the wave height or H_s. Moreover, uncertainties in both H_s and T_p will play a role for the determination of the α_R. This is the drawback of using the response-based alpha-factor. However, based on the same procedure for estimating the extreme responses in Section 3.5, one can inversely identify the allowable sea states in which a safe marine operation can be performed by comparing the extreme response with the allowable limit of response. This can also be done when using the forecast sea states and considering the forecast uncertainty.

One example is illustrated in Fig. 17. The solid black line, resulting into the same extreme response, indicates the sea state limit under which a safe marine operation can be performed when a certain allowable response limit R_E^0 is used. For instance, at the point A, R_E^A, which is the characteristic value of the response under the actual sea state (H_s^A, T_p^A), is equal to the allowable limit R_E^0. Therefore, the black curve represents the allowable sea states of the operation and should be used in the comparison with the forecast sea states for decision-making.

This is the case without considering the uncertainty in forecast sea states. If forecast uncertainty of this sea state at a certain lead time (e.g., 3 h) is considered, the actual sea state should be described by the distribution $f_{H_s^t T_p^t | H_s^f T_p^f}(h_s^t, t_p^t | h_s^f, t_p^f)$ instead of a single value,

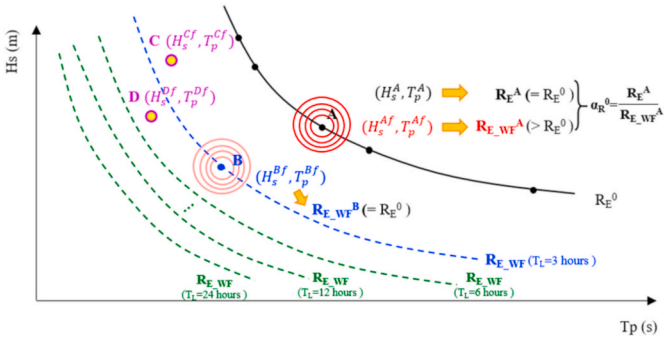

Fig. 17. Schematic outline of allowable sea state assessment considering weather forecast uncertainty.

which is represented by the red circles around the point A. In this case, the characteristic value $R^{A}_{E\_WF}$, calculated by Eqs. (36) and (37), is larger than R^{A}_{E}. The ratio is the α_R with respect to this sea state and forecast lead time. This implies that if the sea state forecast uncertainty is included, the extreme response will larger than the allowable response limit and the operation cannot be safely performed for this forecasted sea state $(H_s^{Af},\ T_p^{Af})$. Therefore, the sea state should be reduced to a certain level to ensure that the characteristic value of the extreme response can be equal to the same allowable response limit. For example, at the point B, it is found that the characteristic value $R^{B}_{E\_WF}$, corresponding to the forecasted sea state $(H_s^{Bf},\ T_p^{Bf})$ with the lead time of 3 h, is equal to the allowable response limit R^{0}_{E}. As a result, this point is along the allowable sea states considering sea state forecast uncertainty.

By performing the same calculation for various forecasted sea states, allowable sea states including the uncertainty in sea state forecasts at different forecast lead times can be produced. These are plotted as blue and green dash lines. All these curves need to be provided for the use in real marine operations, and compared with sea state forecasts to support decision-making during the execution phase. For instance, if a 3 h-ahead forecasted sea state is $(H_s^{Cf},\ T_p^{Cf})$, by checking its location in Fig. 17 (that is at the point C), one can conclude that the operation cannot be executed since it is above the blue line. By contrast, if the 3 h-ahead forecasted sea state is $(H_s^{Df},\ T_p^{Df})$ which is below the blue line, the operation is considered executable.

Followed by this procedure, the allowable sea states in terms of the crane tip motion are assessed. This is done by comparing the characteristic values of the crane tip motion with the corresponding allowable limits for each sea state. Regarding the allowable limit of response, it is normally estimated based on structural damage criteria and reasonable assumptions. In this study, the allowable limits are simply assumed to be constant values. Figs. 18 and 19 illustrate the allowable sea states with 10^{-4} and 10^{-2} exceedance probabilities, and the corresponding allowable limits of the crane tip motion in Y_c direction are assumed to be 0.8 m and 0.4 m respectively. For each selected exceedance probability, results based on TSML and PBML methods are parallelly provided.

Similar to the description in Fig. 17, the line in Figs. 18 and 19 represents the maximum allowable sea states, and all sea states below the line are feasible. The black solid line denotes allowable sea state limits that does not include weather forecast uncertainty. The dash lines in different colors are allowable sea states considering forecast uncertainties at different lead times.

It is visible that by adopting the response-based alpha-factor method, allowable sea states at different lead times can be generated, which is convenient to assist decision-making during the execution of installation operation. As displayed, there is a significant difference in the allowable sea states when the uncertainty in sea state forecast is included. In addition, the allowable sea states gradually decrease as the forecast lead time increases. The forecast uncertainties induced by the two methods (i.e. TSML and PBML) also result in different allowable sea states.

According to the allowable sea states, workable weather windows can further be identified by comparing the weather forecasts with allowable sea states. The allowable sea states shown in Fig. 18 (a) are utilized and taken as an example for illustration. The forecasted time series and identified weather windows in one year are shown in Fig. 20. The weather windows based on the alpha-factor method are also provided as a reference. Given that uncertainties related to T_p forecasts are not taken into account in the alpha-factor method, two marginal cases are considered. Since all sea states along the solid line in Fig. 18 (a) are allowable sea states correspond to the allowable limit, there are series critical couples of the H_s and T_p. In this study, the H_s of 4 m and 2.3 m are utilized, corresponding to the maximum and minimum T_p (i.e., 7.2 s and 10 s). The related α-factors are estimated following the method proposed by DNV, on the basis of H_s forecasts generated by the TSML method at the North Sea center.

Fig. 20 (a) shows the continuous forecasted time series of H_s and T_p in a year by the TSML method, which are one-day-ahead forecasts starting from 0 o'clock every day and all one-day-ahead forecasts are linked end to end. Fig. 20 (b) shows the comparison result between the weather forecasts and the allowable sea states based on the response-based alpha-factor method. The green part is the time period that weather forecasts in terms of H_s and T_p are lower than the allowable sea states, indicating that the operation can be executed safely. Otherwise, the operation is unsafe, represented by the red part. Meanwhile, Fig. 20 (c) and (d) show the similar results based on the alpha-factor method, where the operational limits in terms of H_s are 4 m and 2.3 m, respectively. A large difference can be seen from the subfigures (c) and (d), indicating that the uncertainty related forecasts of T_p has a significant influence on the weather windows. Hence, it is necessary to consider wave period forecast uncertainty in marine operations, at least for the operations applying floating crane vessels. In comparison, subfigure (b) can give more reliable weather windows, by including forecast uncertainties in T_p

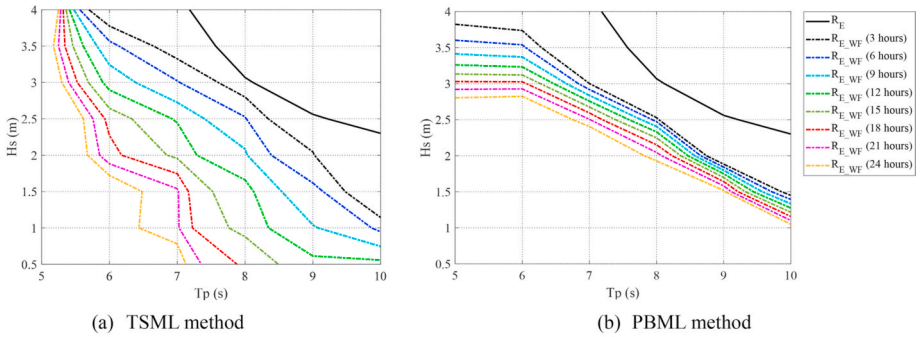

(a) TSML method (b) PBML method

Fig. 18. Allowable sea states of the crane tip motion (allowable limit = 0.8 m, 10^{-4} exceedance probability) (a) TSML method (b) PBML method.

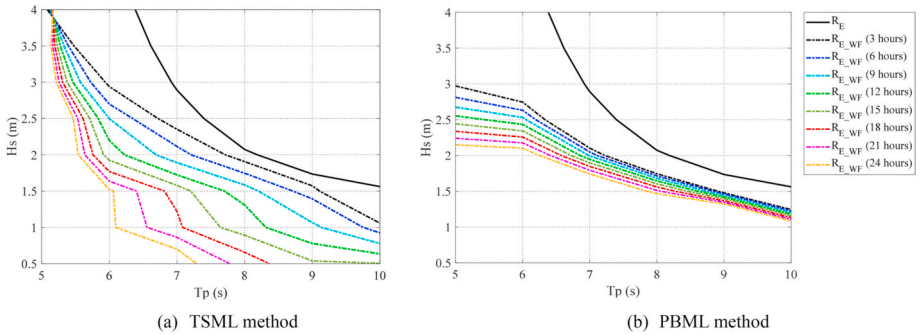

(a) TSML method (b) PBML method

Fig. 19. Allowable sea states of the crane tip motion (allowable limit = 0.4 m, 10–2 exceedance probability) (a) TSML method (b) PBML method.

(a) Forecasted sea state time series

(b) Weather windows estimation (with response-based alpha-factor)

(c) Weather windows estimation (with alpha-factor, $H_{s\_lim} = 4$ m)

(d) Weather windows estimation (with alpha-factor, $H_{s\_lim} = 2.3$ m)

Fig. 20. Effect of weather forecast uncertainty on weather windows estimation (crane tip motion, TSML method) (a) Forecasted sea state time series (b) Weather windows estimation (with response-based alpha-factor) (c) Weather windows estimation (with alpha-factor, $H_{s\_lim} = 4$ m) (d) Weather windows estimation (with alpha-factor, $H_{s\_lim} = 2.3$ m).

together with H_s into dynamic response analysis, allowable sea states assessment as well as weather windows identification.

Overall, application of the response-based alpha-factor method on allowable sea states assessment as well as weather windows identification is preliminary illustrated in this section. An important but simple parameter, the crane tip motion, in the blade installation of offshore wind turbine is discussed as an example by numerical simulation in frequency domain. Advantages of this new proposed method is shown by a comparison with the alpha-factor method.

5. Conclusions

In this study, a methodology for developing a response-based correction factor (called the response-based alpha-factor α_R) is proposed for the use in assessing allowable sea states for marine operations, with emphasis on accounting for the effect of weather forecast uncertainty. It comprises three main parts, namely quantification of the weather forecast uncertainty, statistical analysis of structural dynamic responses of coupled system for marine operations and allowable sea states assessment by means of response-based criteria. Based on the methodology, the α_R can be derived for a specific operation, which is similar as the α-factor proposed by DNV but can reflect the effect of forecast uncertainties of both H_s and T_p on the dynamic response of offshore structures. It should be noted that the forecast uncertainty of other weather variables (such as wave direction D_u and mean wind speed U_w) can also be included in the method if necessary. Then, the allowable sea states accounting for the weather forecast uncertainty for the operation can be assessed at different forecast lead times. By comparing the allowable sea states with weather forecasts, workable weather windows can be identified and selected, which is a better reference for the decision-making in the execution phase.

A case study regarding the blade installation of offshore wind turbine by a semi-submersible crane vessel is carried out to illustrate the procedure and show the usage of the proposed α_R. In the paper, crane tip motion is considered and regarded as the operational limiting response parameter. Following the proposed method, uncertainties inherent in H_s and T_p forecasts generated by the TSML and PBML methods at the North Sea center are quantified first. Then, based on the characteristic values evaluated by the probabilistic analysis of dynamic responses with and without weather forecast uncertainty, α_R factors are established for various sea states. The corresponding allowable sea states are then assessed, and the workable weather windows are finally identified and selected. Results indicate that forecast uncertainties in both H_s and T_p are important, and compared to the α-factor, the α_R can take into account them more comprehensive and reflects their effect on the crane tip motion. Overall, this case study demonstrates that the proposed method can provide an effective and reliable way to assess the allowable sea states of the operation considering weather forecast uncertainty and further assist in operation decision-making.

However, it should be emphasized that the case study only deals with the motion response of the crane tip under wave conditions, to illustrate the feasibility of the proposed method. In practice, in addition to the wave loads, the nonlinear wind loads acting on the blade are important during the blade installation. Correspondingly, the limiting response parameter related to the blade motion and the influences of coupled wind and waves on the installation system should be considered. The effect of weather forecast uncertainty on the entire blade installation process will be addressed using the proposed method in time domain in the near future.

Declaration of competing interest

The authors declare that they have no known competing financial interests or personal relationships that could have appeared to influence the work reported in this paper.

Acknowledgments

This work was supported by the Center for Marine Operations in Virtual Environments (MOVE) and Centre for Autonomous Marine Operations and Systems(AMOS), at the Department of Marine Technology, NTNU, Trondheim, Norway. The support is gratefully acknowledged by the authors.

References

[1] Commission EE. Clean energy for all Europeans, vol. 2016. COM; 2016. p. 860.
[2] Bilgili M, Yasar A, Simsek E. Offshore wind power development in Europe and its comparison with onshore counterpart. Renew Sustain Energy Rev 2011;15:905–15.
[3] Dnv G. DNV-OS-H101: marine operations. General, Offshore Standard 2011.
[4] Guachamin-Acero W, Li L, Gao Z, Moan T. Methodology for assessment of the operational limits and operability of marine operations. Ocean Eng 2016;125:308–27.
[5] Li L, Guachamin-Acero W, Gao Z, Moan T. Assessment of allowable sea states during installation of offshore wind turbine monopiles with shallow penetration in the seabed. J Offshore Mech Arctic Eng 2016;138.
[6] Guachamin-Acero W, Moan T, Gao Z. Steady state motion analysis of an offshore wind turbine transition piece during installation based on outcrossing of the motion limit state. In: ASME 2015 34th International Conference on ocean, offshore and Arctic Engineering. American Society of Mechanical Engineers Digital Collection; 2015.
[7] Guachamin-Acero W, Gao Z, Moan T. Methodology for assessment of the allowable sea states during installation of an offshore wind turbine transition piece structure onto a monopile foundation. J Offshore Mech Arctic Eng 2017;139.
[8] Guachamin-Acero W, Gao Z, Moan T. Numerical study of a novel procedure for installing the tower and rotor nacelle assembly of offshore wind turbines based on the inverted pendulum principle. J Mar Sci Appl 2017;16:243–60.
[9] Ahn D, Shin S-c, Kim S-y, Kharoufi H, Kim H-c. Comparative evaluation of different offshore wind turbine installation vessels for Korean west–south wind farm. International Journal of Naval Architecture and Ocean Engineering 2017;9:45–54.
[10] Dalgic Y, Lazakis I, Dinwoodie I, McMillan D, Revie M. Advanced logistics planning for offshore wind farm operation and maintenance activities. Ocean Eng 2015;101:211–26.
[11] O'Connor M, Burke D, Curtin T, Lewis T, Dalton G. Weather windows analysis incorporating wave height, wave period, wind speed and tidal current with relevance to deployment and maintenance of marine renewables. In: Proceedings of the 4th International Congress on ocean energy. Ireland: Dublin; 2012. p. 17–9.
[12] Group TW. The WAM model—a third generation ocean wave prediction model. J Phys Oceanogr 1988;18:1775–810.
[13] Booij N, Ris RC, Holthuijsen LH. A third-generation wave model for coastal regions: 1. Model description and validation. J Geophys Res: Oceans 1999;104:7649–66.
[14] Tolman HL. A third-generation model for wind waves on slowly varying, unsteady, and inhomogeneous depths and currents. J Phys Oceanogr 1991;21:782–97.
[15] Fusco F, Ringwood JV. Short-term wave forecasting with ar models in real-time optimal control of wave energy converters. IEEE International Symposium on Industrial Electronics, vol. 2010. IEEE; 2010. p. 2475–80.
[16] Pena-Sanchez Y, Ringwood JV. A critical comparison of AR and ARMA models for short-term wave forecasting. Proc 12th Eur Wave Tidal Energy Conf2017. p. 9611-.9616.
[17] Ge M, Kerrigan EC. Short-term ocean wave forecasting using an autoregressive moving average model. UKACC 11th International Conference on Control (CONTROL), vol. 2016. IEEE; 2016. p. 1–6.
[18] Kamranzad B, Etemad-Shahidi A, Kazeminezhad M. Wave height forecasting in dayyer, the Persian gulf. Ocean Eng 2011;38:248–55.
[19] Adytia D, Yonanta AR, Subasita N. Wind wave prediction by using autoregressive integrated moving average model: case study in jakarta bay. Int J Inf Commun Technol 2019;4:33–42.
[20] Deo M, Naidu CS. Real time wave forecasting using neural networks. Ocean Eng 1998;26:191–203.
[21] Deo MC, Jha A, Chaphekar A, Ravikant K. Neural networks for wave forecasting. Ocean Eng 2001;28:889–98.
[22] Mandal S, Rao S, Raju D. Ocean wave parameters estimation using backpropagation neural networks. Mar Struct 2005;18:301–18.
[23] Malekmohamadi I, Bazargan-Lari MR, Kerachian R, Nikoo MR, Fallahnia M. Evaluating the efficacy of SVMs, BNs, ANNs and ANFIS in wave height prediction. Ocean Eng 2011;38:487–97.
[24] Mandal S, Prabaharan N. Ocean wave forecasting using recurrent neural networks. Ocean Eng 2006;33:1401–10.

[25] Sadeghifar T, Nouri Motlagh M, Torabi Azad M, Mohammad Mahdizadeh M. Coastal wave height prediction using recurrent neural networks (RNNs) in the south caspian sea. Mar Geodes 2017;40:454–65.
[26] Özger M, Şen Z. Prediction of wave parameters by using fuzzy logic approach. Ocean Eng 2007;34:460–9.
[27] Akpınar A, Özger M, Kömürcü MI. Prediction of wave parameters by using fuzzy inference system and the parametric models along the south coasts of the Black Sea. J Mar Sci Technol 2014;19:1–14.
[28] Stefanakos C. Fuzzy time series forecasting of nonstationary wind and wave data. Ocean Eng 2016;121:1–12.
[29] Wu M, Stefanakos C, Gao Z, Haver S. Prediction of short-term wind and wave conditions for marine operations using a multi-step-ahead decomposition-ANFIS model and quantification of its uncertainty. Ocean Eng 2019;188:106300.
[30] Jip D. Technical report. Marine operation Rules, Revised alpha factor—joint industry project. Oslo: DNV; 2007.
[31] Wilcken S. Alpha factors for the calculation of forecasted operational limits for marine operations in the Barents Sea. Norway: University of Stavanger; 2012.
[32] Gintautas T, Sørensen JD. Improved methodology of weather window prediction for offshore operations based on probabilities of operation failure. J Mar Sci Eng 2017;5:20.
[33] Wu M, Stefanakos C, Gao Z. Multi-step-ahead forecasting of wave conditions based on a physics-based machine learning (PBML) model for marine operations. J Mar Sci Eng 2020;8:992.
[34] Uppala SM, Kållberg P, Simmons A, Andrae U, Bechtold VDC, Fiorino M, et al. The ERA-40 re-analysis. Q J R Meteorol Soc: A j. atmos. sci., appl. meteorology and phys. oceanography 2005;131:2961–3012.
[35] Dee DP, Uppala S, Simmons A, Berrisford P, Poli P, Kobayashi S, et al. The ERA-Interim reanalysis: configuration and performance of the data assimilation system. Q J Roy Meteorol Soc 2011;137:553–97.
[36] Hersbach H, Dee D. ERA5 reanalysis is in production. ECMWF newsletter 2016;147:5–6.
[37] Gusdal Y, Carrasco A, Furevik B, Sætra Ø. Validation of the operational wave model WAM at met. No-report 2010. Report of the Norvegian Meteorological Institute-Oceanography 2011;8. no 14/2011, December.
[38] Saha S, Moorthi S, Pan H-L, Wu X, Wang J, Nadiga S, et al. The NCEP climate forecast system reanalysis. Bull Am Meteorol Soc 2010;91:1015–58.
[39] Li L, Gao Z, Moan T. Joint distribution of environmental condition at five european offshore sites for design of combined wind and wave energy devices. J Offshore Mech Arctic Eng 2015;137.
[40] Laloyaux P, de Boisseson E, Balmaseda M, Bidlot JR, Broennimann S, Buizza R, et al. CERA-20C: a coupled reanalysis of the Twentieth Century. J Adv Model Earth Syst 2018;10:1172–95.
[41] Lee C-H, Newman JN. WAMIT User manual. WAMIT, Inc.; 2006. p. 42.
[42] Dnv G. Sesam user manual-Wadam. DNV GL Software; 2017.
[43] Haver S. Metocean modelling and prediction of extremes. Lecture notes in TMR4195-design of offshore structures Department of marine Technology. Norwegian University of Science and Technology; 2017.
[44] Zhao Y, Cheng Z, Gao Z, Sandvik PC, Moan T. Numerical study on the feasibility of offshore single blade installation by floating crane vessels. Mar Struct 2019;64:442–62.
[45] Jiang Z, Gao Z, Ren Z, Li Y, Duan L. A parametric study on the final blade installation process for monopile wind turbines under rough environmental conditions. Eng Struct 2018;172:1042–56.
[46] Zhao Y, Cheng Z, Sandvik PC, Gao Z, Moan T. An integrated dynamic analysis method for simulating installation of single blades for wind turbines. Ocean Eng 2018;152:72–88.
[47] Zhao Y, Cheng Z, Sandvik PC, Gao Z, Moan T, Van Buren E. Numerical modeling and analysis of the dynamic motion response of an offshore wind turbine blade during installation by a jack-up crane vessel. Ocean Eng 2018;165:353–64.
[48] Verma AS, Jiang Z, Gao Z, Vedvik NP. Effects of a passive tuned mass damper on blade root impacts during the offshore mating process. Mar Struct 2020;72:102778.
[49] Wu M, Gao Z, Stefanakos C, Haver S. Comparison of machine-learning methods for multi-step-ahead prediction of wave and wind conditions. 2019. p. 1074–93.
[50] Veritas DN. Recommended practice DNV-RP-C205: environmental conditions and environmental loads. DNV, Norway; 2010.